POLYMER ORGANIC SOLAR CELLS

Phua Hao Yu

A0086715X

A THESIS SUBMITTED IN PARTIAL FULFILLMENT TOWARDS

THE BACHELOR OF SCIENCE (HONORS) IN PHYSICS

DEPARTMENT OF PHYSICS

NATIONAL UNIVERSITY OF SINGAPORE

2015

Acknowledgements

I would like to thank A/Prof Peter Ho, Asst/Prof Chua Lay-Lay and Dr Rachael Png Ruiqi for accommodating me in the Organic Nano Device Lab.

My heartfelt gratitude to Jun Kai for taking time to guide me in both theoretical and experimental aspects of this study. For tolerating my shenanigans and not turning into a disciplinarian, which turned out more for the better, while still giving out reprimands and encouragements whenever necessary. Thank you for teaching me skills beyond the classroom and for making the journey a pleasant one.

In the midst of this, we mourn the passing of Mr Lee Kuan Yew.

Thank you to Rachael for taking time out of her now even more busy schedule to review this work.

And to the rest of ONDL for their guidance in times of trouble and aid that made this work possible. I am appreciative of the warmth received from the members of ONDL and the cleanroom.

I would also like to thank my family and friends for the support they provided.

Abstract

Organic photovoltaics possess many qualities that are rarely available in inorganic photovoltaics, namely its ability for high absorbance, flexibility, cheap and high throughput processing. While electron donor polymers are many aplenty, electron acceptor polymers with high electron mobility are just introduced to the stage and competes with fullerene derivatives that has its long standing reputation as the acceptor material of choice. In the other corner, morphology plays an important factor influencing PCE of an organic solar cell. Bulk heterojunctions of organic solar cells are usually formed from spontaneously demixed biblends of the active layer solution and removes control from the hands of the investigator. Many efforts were made to wrestle control back but these still relied on the spontaneous demixing of the solution. In this study, a crosslinked donor matrix structure is employed to create a controllable morphology of donor polymers which is then filled and back-infiltrated with acceptor materials. We demonstrate that a crosslinked back-infiltrated solar cell improve in performance over a demixed biblend. However, this method showed some dependence on the donor material involved, hence requires some tailoring for optimal adoption. Devices with small molecule back-infiltrated sets the amount of infiltration that might optimally occur and were closely matched by low molecular weight polymers but not by high molecular weight polymers. As mobility is dependent on molecular weight, this balance is identified as one of the parameters that requires optimising. Device parameter of Voc was observed to increase over all device tested and this notable effect should be studied in greater detail and could lend to a clearer picture of the morphology in a crosslinked back-infiltrated active layer.

Table of Contents

Acknowledgements iii
Abstract iv
Table of Contents v
1. Introduction 1
1.1 Solar energy 1
1.2 Organic solar cells 1
1.3 Mechanism of photocurrent generation 2
1.4 Bulk heterojunction 4
1.5 Crosslinked polymer-donor network cells 5
1.6 Motivation 6
2. Characterisation techniques 7
2.1 Materials 7
2.1.1 P3HT and PCBM 7
2.1.2 PNDI 8
2.1.3 PBDTTPD 9
2.2 Single-carrier diode fabrication and characterisation techniques 9
2.2.1 Single-carrier diode fabrication 9
2.2.2 Space charge limited current mobility 11
2.3 Solar cell fabrication and characterisation technique 12
2.3.1 Solar cell fabrication 12
2.3.2 Solar simulation 13
2.3.3 Device characterization 14
2.3.4 Photoluminescence measurements 15
3. Results and discussions 18
3.1 Photoluminescence 18
3.2 Device characteristics 18
3.2.1 Characteristics of crosslinked donor matrix 18
3.2.2 P3HT:PCBM 20
3.2.3 P3HT:PNDI 23
3.2.4 PBDTTPD:PCBM 26
3.2.5 PBDTTPD:PNDI 29
3.3 Semiconducting behaviour of PNDI on molecular weight 31
3.4 Symmetricity 32

4. Conclusion 34
5. References 35
6. Appendix 37

1. Introduction

1.1 Solar energy

Energy is one of the most important factor that places a ceiling on social development. In the past two millennia, societies have collapsed when their development met with that ceiling but were unable to break through[1]. Only with the discovery and efficient extraction of energy from fossil fuels was social development able to break the ceiling. Now faced with the pressing issue of climate change, our options of using fossil fuels to satisfy our ever-increasing energy consumptions are dwindling. Solar, wind and wave provide an alternative source of clean and renewable energy that solves the problems of limited energy reserves and excessive carbon dioxide emission. Of more importance is solar, which drives the winds and the waves, and also more easily accessible.

Thanks to the continuous effort put into the research and development of photovoltaics (PV), the levelised cost of energy (LCOE), which is calculated as the total cost of plants and equipment over total energy production (kWh) during effective lifetime, has steadily fallen at an average rate of 13% since 2006[2]. On the other hand, the price of electricity from conventional sources have steadily risen over the years. Grid parity is said to be achieved when the LCOE equals or falls below the market price of electricity and reaching it will result in the adoption of this new technology that can sweep across entire nations. Since 2012, the PV power has reached grid parity[2] in Germany and following the trends of energy prices, many more countries will achieve grid parity. However, in order to replace coal, the LCOE of PV power has to fall even further and research and development to push the efficiency of solar cells must continue.

1.2 Organic solar cells

The discovery of organic semiconductors in the 1950s[3] led to research into the new field of organic solar cells. Polymers offer certain advantages over inorganic materials, such as strong absorption coefficients in the visible spectrum, which allows for thinner material layers to be used, leading to devices that have the potential to be both light and flexible. The relationship between polymer chain length and side chains to their energetic behaviours also provided the

possibility of tailoring such materials to specific needs, opening a huge playing field for researchers.

Although being a semiconducting material, the charge carrier mobilities of organic semiconductors are much lower than that of inorganic materials, appropriately, their power conversion efficiencies are also lower and are still lagging behind inorganic solar cells today. Degradation of the device also occurs much faster in organic solar cells, giving them a lifespan of around 15 years compared to inorganic's 25 years[4].

However, cost of producing organic materials are more favourable over inorganic materials, where high temperatures are required, while the cost-effectiveness of device fabrication are also more favourable for organic solar cells, with the possibility of employing high throughput inkjet printing or roll-to-roll solution processing thus easing the way into commercialising.

1.3 Mechanism of photocurrent generation

Organic semiconductors typically have low relative permittivity (or dielectric constants) in contrast to the higher relative permittivity of inorganics. As a consequence, the excitons formed in organic semiconductors during the absorption of a photon tend to be Frenkel excitons, with binding energies[5] of 0.5 – 1 eV. Thermal energies at a room temperature of 298K reaches 0.025eV which is much lower than the binding energy of the excitons, hence investigations towards efficient dissociation of the exciton led to a requirement of at least a 0.3 eV difference between energy levels at the donor-acceptor interface[6]. Another important difference between organic and inorganic semiconductors is its exciton diffusion length, which due to its short lifetime, its diffusion length in an organic semiconductor is only around 10 nm[7].

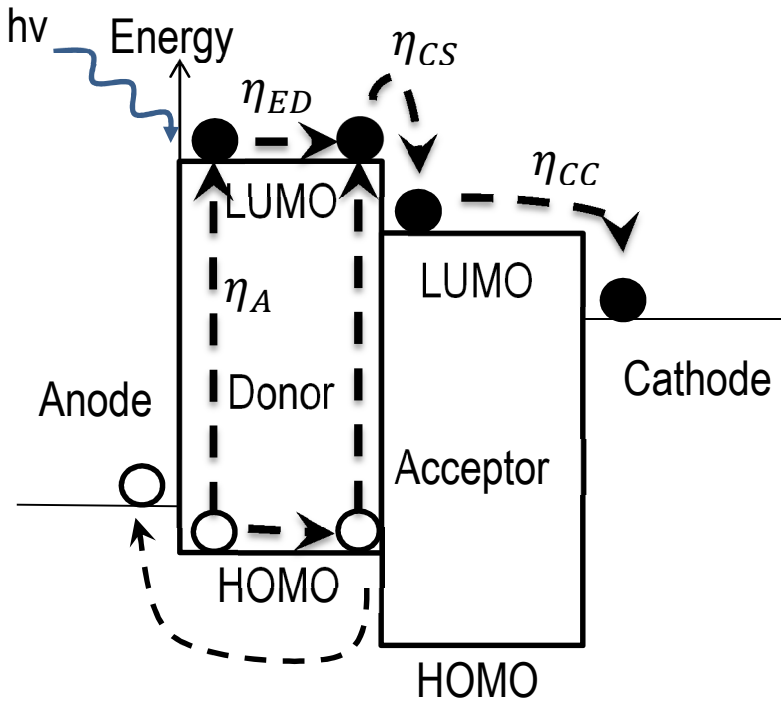

Figure 1: Fundamental processes of photon to electron conversion in an organic solar cell.

The four fundamental step of photocurrent generation in an organic solar cells is illustrated in figure 1. First, a photon is absorbed by the active layer which excites an electron from the highest occupied molecular orbital (HOMO) level to the lowest unoccupied molecular orbital (LUMO) level, generating a Frenkel exciton. The efficiency at which the exciton is generated from the incident photons is termed the absorption efficiency (η_A). Second, to dissociate into free charge carriers, the exciton must diffuse to the donor-acceptor interface and survive long enough to reach the interface. Due to the short diffusion length of the excitons, the thickness of the material phases greatly factors into the exciton diffusion efficiency (η_{ED}), the ratio of excitons reaching the interface to the number of excitons generated. Third, upon reaching the donor-acceptor interface, a charge transfer occurs in the exciton where an electron from the donor gets transferred to the acceptor or a hole from the acceptor to the donor[8]. The efficiency of this charge transfer occurrence is termed the charge separation efficiency (η_{CS}). Lastly, the charge carriers of the exciton, in the presence of the built-in electric field, is finally able to dissociate into free charge carriers and travel through their respective material to be collected at the electrodes. The ratio of number of charge carriers collected to the number of charge transfer occurrence is termed the charge collection efficiency (η_{CC}). The external quantum efficiency (EQE) measures the ratio of incident photon converted to collected charge carriers and is represented as

$$EQE = \eta_A \cdot \eta_{ED} \cdot \eta_{CS} \cdot \eta_{CC} \quad (1)$$

while the internal quantum efficiency (IQE) measures the ratio of exciton generated to collected charge carriers and is represented as

$$IQE = \eta_{ED} \cdot \eta_{CS} \cdot \eta_{CC} \quad (2)$$

1.4 Bulk heterojunction

The development of organic solar cells started off with the familiar bilayer structure employed by inorganics. While their high absorption coefficients allows them to be thin, the effective absorption thickness of polymers are still around 50-300nm. In addition to that, the hugely limited diffusion length (10nm) of the exciton means a bilayer at effective light absorption thickness would do a poor job at extracting these energies. This was realized as early as 1986 where the state of the art bilayer organic solar cell[9] attained a PCE of 1%.

A breakthrough in morphology development came about when Yu et al.[10] created a bulk heterojunction (BHJ) morphology that solved many issues that frustrated attempts for organic materials to become viable options in solar cell development. This new morphology, as shown in figure 2, had material phases that were separate from each other at a length scale of only 5-50nm and provided many more times the area of donor-acceptor interfaces. Excitons in organic materials, with their short diffusion length, are now able to successfully reach the interfaces to dissociate into free charge carriers. Efficiencies of organic solar cells saw a marked increase with this simple yet elegant solution and PCEs have reached 4.24%[11]. However, this new method also brought about new problems, such as the difficulty in controlling how the morphology would form. Having control over the morphology is essential, for if the phase separation is too thin, isolated domains will form where the charge carriers cannot reach the electrodes while if it is too thick, excitons cannot reach the interfaces.

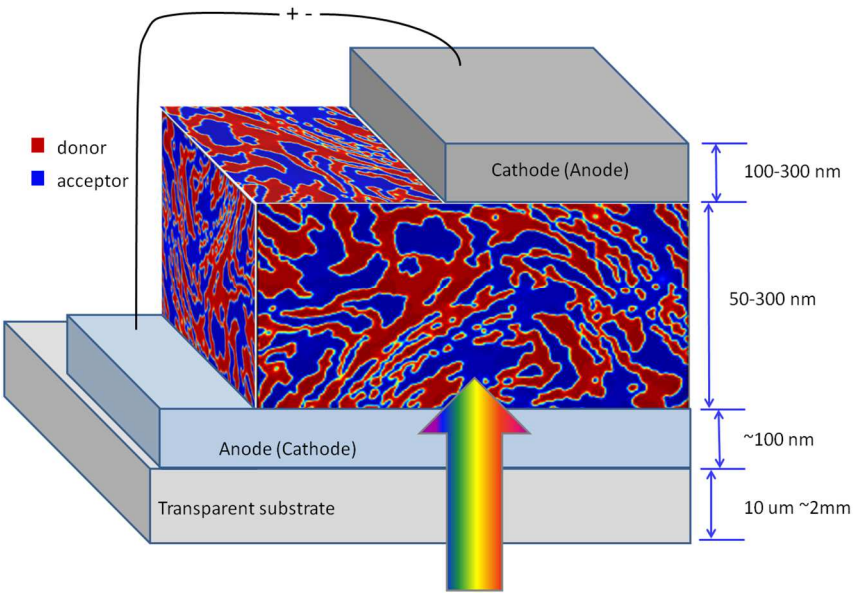

Figure 2: Schemetic diagram of a bulk heterojunction solar cell. A typical structure is glass/130 nm ITO/50 nm PEDT:PSSH/Active Layer/30 nm Ca/120 nm Al

1.5 Crosslinked polymer-donor network cells

Crosslinkers are molecules that are able to bind, on both ends, to polymers. Developed and produced in-house[12], sterically hindered bis(fluorophenyl azide) (sFPA) provides advantages through its non-specific crosslinking mechanism (figure 3), allowing a much lower concentration to achieve high retention rates. These crosslinkers are also tuned to be activated at the deep ultraviolet (DUV) region (254 nm), which is not readily absorbed by the donor polymers, hence allowing for photoactivation of the crosslinkers deep into the material film. After photoactivation, the crosslinked polymer film is washed with solvent to give a sponge-like matrix which is resistant to further dissolution. On the other hand, this polymer matrix swells upon contact with appropriate solvents, allowing for other polymers and molecules to be back-infiltrated into the matrix to create a bulk heterojunction.

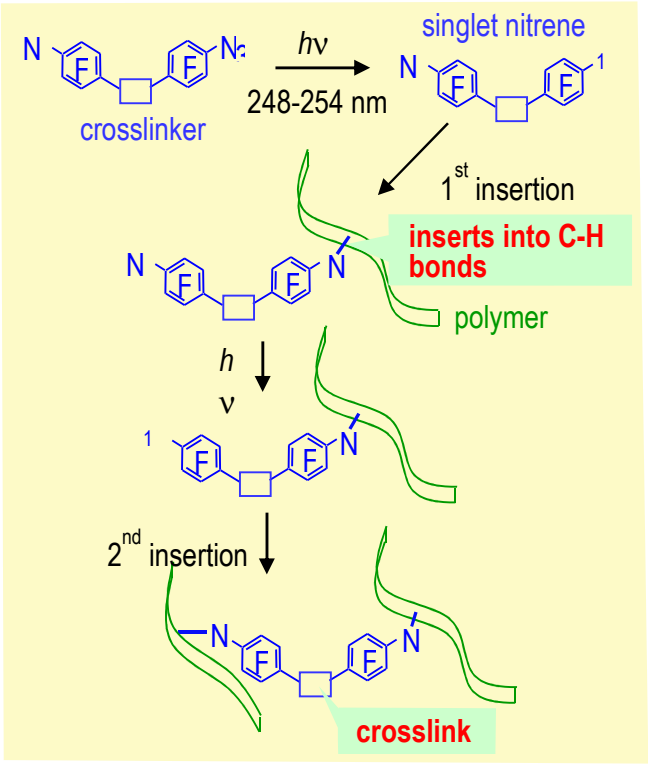

Figure 3: Schematic diagram of crosslinking process. The singlet nitrene inserts into the C-H bonds upon deep ultraviolet photoactivation.

In organic solar cells, this translate to the ability of creating a polymer matrix for use with the method of back-infiltration. This method is able to create near ideal percolation[13] pathways without resorting to coarsening phase separation, allowing efficient extraction of free charge carriers to their respective electrode while maintaining a fine phase separation and allowing for efficient exciton diffusion to the interface. Such a control of the morphology also does away with the need to coarsen phase separation for the purpose of suppressing the formation of isolated domains. This method of crosslinking and back-infiltration solves many of the issues that plagued demixed biblend BHJs but new challenges have arisen, including the extent of effects crosslinkers have on material properties and the morphologies resulting from back-infiltration with acceptor polymers, which this work will endeavour to investigate.

1.6 Motivation

A fine phase separation is advantageous for exciton diffusion efficiency but a coarsening of the phase separation is usually used to improve true percolation pathways. Creating an interpenetrating matrix minimises the occurrence of isolated domains without compromising

on the fineness of the phase separation. The method of crosslinking and back-infiltration is relatively new and has been shown to work with small molecules, increasing the performance of the solar cell[13]. Instead of using small molecules, acceptor type polymers can provide the advantage of higher absorption coefficients and tuneable energy levels over fullerene derivatives. This study aims to aid in extending the applications of back-infiltration to the more complex system of polymer-polymer active layers. Through morphological studies and characterisation, the mechanism and limitations of morphology formation and performance is sought to be understood.

2. Characterisation techniques

2.1 Materials

2.1.1 P3HT and PCBM

The donor polymer poly(3-hexylthiophene) (P3HT) and acceptor fullerene derivative phenyl-C61-methylbutyric ester (PCBM) (Figure 4) have been studied extensively for the last 10 years due to their high mobilities of 3.3×10^{-8} $m^2/(Vs)$ and 2.0×10^{-7} $m^2/(Vs)$ respectively[14], with thousands of publication on devices using these two materials[15]. It was the high electron mobility, rarely found in polymers, coupled with an ability to self-assemble, aggregating into the appropriate domain sizes, which made PCBM so attractive, even though they have limited absorption capabilities and are expensive.

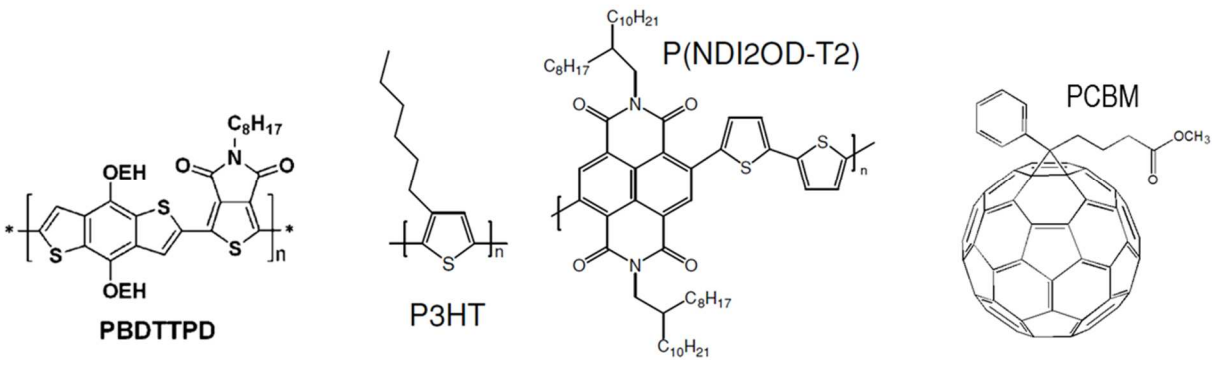

Figure 4: From left to right: donor polymers PBDTTPD and P3HT, acceptor materials PNDI and PCBM.

2.1.2 PNDI

Polymers offer certain advantages over fullerenes, their absorption spectrum can extend to wavelengths longer than what fullerene can reach (figure 5) and their absorption coefficients are higher in the solar radiation spectrum. Their energy levels are tuneable, allowing LUMO levels to be optimised to the device, to achieve the highest Voc while maintaining efficient exciton charge transfer. Also, their viscosity in solutions can be controlled, allowing for more control in the fabrication process and upscaling.

A high-mobility electron-transporting polymer, poly{[N , N ’-bis(2-octyldodecyl)-naphthalene- 1,4,5,8-bis(dicarboximide)-2,6-diyl]-alt-5,5’-(2,2’-bithiophene) (P(NDI2OD-T2)) (PNDI), was successfully fabricated by Yan et al.[16] in 2009 and since then, wide adoptions of this polymer has been made. Space charge limited current (SCLC) electron mobilities for PNDI measures at 3.9×10^{-8} $m^2/(Vs)$, within an order of difference to PCBM. Energy level standings with PCBM compares at a lower LUMO level and a higher HOMO level as shown in figure 6, and the smaller band gap of PNDI is a factor of its better absorption. The absorption spectrum of PNDI also extends into the red region (figure 5) where most of the solar spectrum resides, while PCBM has its absorption spectrum in the ultraviolet region which represents a small fraction of the solar spectrum.

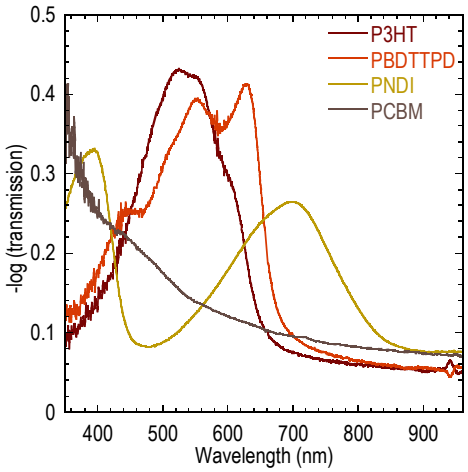

Figure 5: UV-vis spectrums of P3HT, PBDTTPD, PNDI and PCBM pure films.

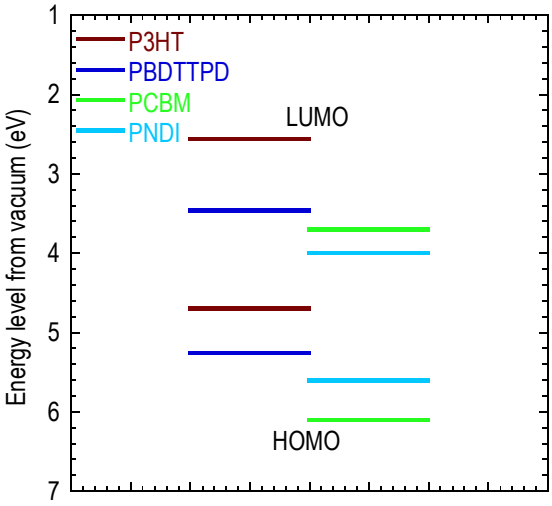

Figure 6: Energy levels of materials of P3HT, PBDTTPD, PNDI and PCBM. The energy gaps between the LUMO of the acceptor and HOMO of donor gives an upper ceiling for Voc for the devices P3HT:PCBM (1.0 V), P3HT:PNDI (0.7 V), PBDTTPD:PCBM (1.56 V) and PBDTTPD:PNDI (1.26 V).

2.1.3 PBDTTPD

In 2010, Zou at al.[17] created a new copolymer with BDT and TPD units, fashioned towards reducing the band gap to between 1.2 and 1.9 eV to maximise range of absorption spectrum, while lowering the HOMO to maximise Voc. Both of these parameters were able to surpass P3HT (figure 6). The absorption spectrum of Poly(benzodithiophene 5-octylthieno[3,4-c] pyrrole-4,6-dione) (PBDTTPD) was also reaching beyond the boundaries of P3HT (figure 5). The SCLC hole mobility of PBDTTPD was, however, at 2.9×10^{-8} $m^2/(Vs)$ an order lower than that of P3HT but not dissimilar to other small band gap polymers[18].

2.2 Single-carrier diode fabrication and characterisation techniques

2.2.1 Single-carrier diode fabrication

A glass slide (1.2cm by 1.2cm) with a rectangular strip of Indium tin oxide (ITO) (1.2cm by 0.8cm) is wash with acetone and isopropyl alcohol (IPA) to remove the photoresist. Cleaning of the substrates was conducted with standard cleaning 1 (SC1) procedure, where the substrates

were cleaned in a solution of 100 ml purified water, 20 ml of hydrogen peroxide and 5 ml of ammonia, and left at 120°C for 45 min. The substrates were then removed and washed with IPA to remove SC1 solution. The substrates were put in oxygen plasma for 10 min to remove any remaining organic material on the surface of the ITO and brought out and left to cool for 10 min. The appropriate PEDT was spun on a spin coater to a thickness of 50 nm. For hole-only diodes, PEDT:PSSH was used. While for electron-only diode, the electron injecting layer of PEDT:PSSCs was used. The substrates were brought into the glove box with a nitrogen environment and baked at 140°C for 10 min to remove any water present. The appropriate donor or acceptor solution was spun on the substrate to a thickness of above 100 nm (thickness measurements were done separately with the same spin conditions). For films to be crosslinked, the substrates are baked at 90°C for 5 min to remove remaining solvents to prevent crosslinking to solvents. The films were then exposed to DUV (254 nm) for 2 min and washed with the same solvent on the spin coater to remove non-crosslinked polymers. The films were then brought to the evaporation chamber and placed face down onto a mask for eight separate electrodes. Ag was loaded for hole-only diodes and evaporated for 120 nm while Ca and Al were loaded for electron-only diodes and evaporated for 30nm and 120 nm respectively. The device was then loaded into the Rachael chamber (figure 7) to preserve the nitrogen environment around the device, then brought out of the glove box and connected to a Keithley terminal for a voltage sweep to obtain its J-V curve.

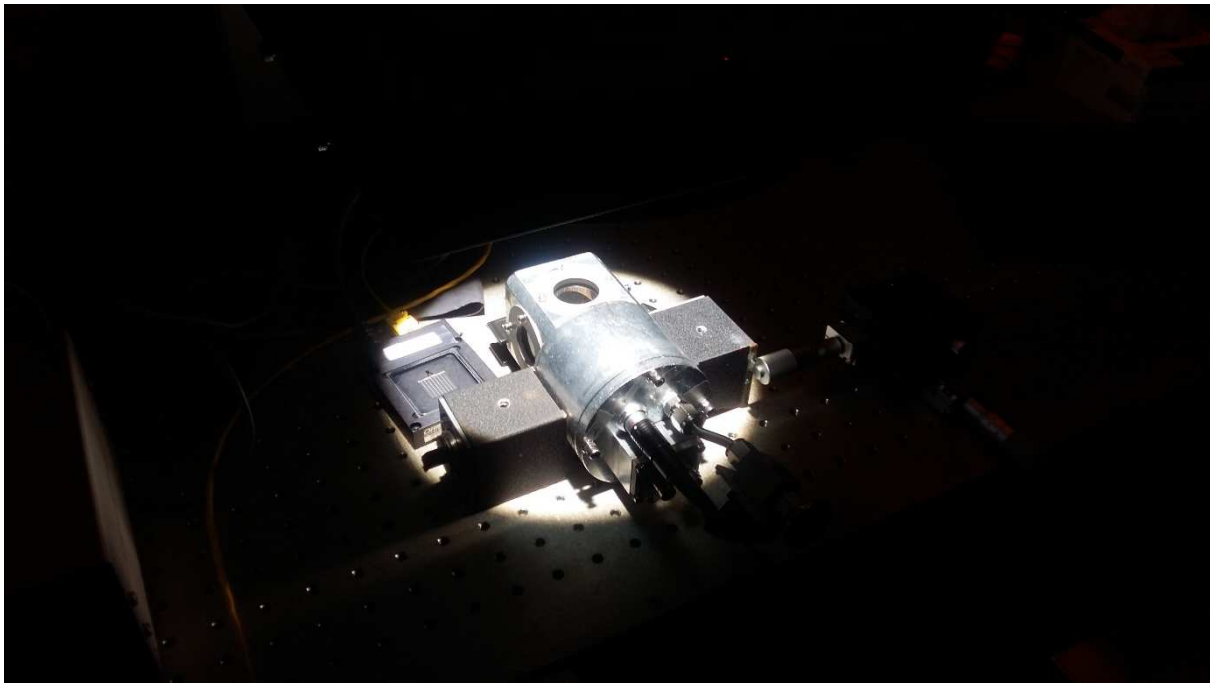

Figure 7: A Rachael chamber in action. Named after Png Ruiqi, Rachael who designed the chamber.

Thin film active layers for ultraviolet-visible (UV-vis) spectroscopy and PL measurements are similarly fabricated on a glass substrate without ITO, PEDT, or metals evaporated.

2.2.2 Space charge limited current mobility

In a dielectric media, excess electrical charges do not rapidly disperse, unlike conductive mediums. Hence they build up in a continuum that is spread out over an area and can slow down like charge carriers due to its repulsive force. Devices requiring SCLC mobility measurements are required to be a single charge carrier type diode. The thickness of the material in question should also be large enough to include a substantial part of the drift region. Mobility is then obtained from fitting the drift region of the J-V curve with the Mott-Gurney law, which deals with thin layers of material

$$J = \frac{9\,\epsilon\,\mu\,V^2}{8\,L^3} \qquad (3)$$

where J is the current density, ϵ the relative permittivity used was 3.5 for polymers, μ the mobility, V the voltage and L the thickness.

2.3 Solar cell fabrication and characterisation technique

2.3.1 Solar cell fabrication

Substrate preparation and cleaning was similar to single-carrier diode fabrication (refer to section 2.2.1). A 50 nm thick layer of PEDT:PSSH was spun onto the substrate on a spin coater. The substrates were brought into the glove box with a nitrogen environment and baked at 140°C for 10 min to remove any water present. For a demixed biblend solution, the active layer is simply spun onto the substrate on a spin coater (figure 8) to the required thickness (around 100 nm). For a crosslinked back-infiltrated device, the donor layer is first spun onto the substrate to a thickness of around 65 nm. The substrates are baked at 90°C for 5 min to remove remaining solvents to prevent crosslinking to solvents. The films were then exposed to DUV (254 nm) for 2 min and washed with the same solvent on the spin coater to remove non-crosslinked polymers. The acceptor solution is then applied onto the crosslinked matrix and a 10 second buffer time is allowed for the swelling of matrix to fully occur. If a volatile solution is used, the spin coater is covered with a dish to reduce the rate of evaporation. The solution is the spun off to the thickness of 50 nm of acceptor material. The films were then brought to the evaporation chamber and placed face down onto a mask for eight separate electrodes Ca and Al were loaded and evaporated for 30nm and 120 nm respectively. The device was then loaded into the Rachael chamber to preserve the nitrogen environment around the device, then brought out of the glove box, placed under a solar simulator (figure 9) and connected to a Keithley terminal for a voltage sweep to obtain its J-V curve.

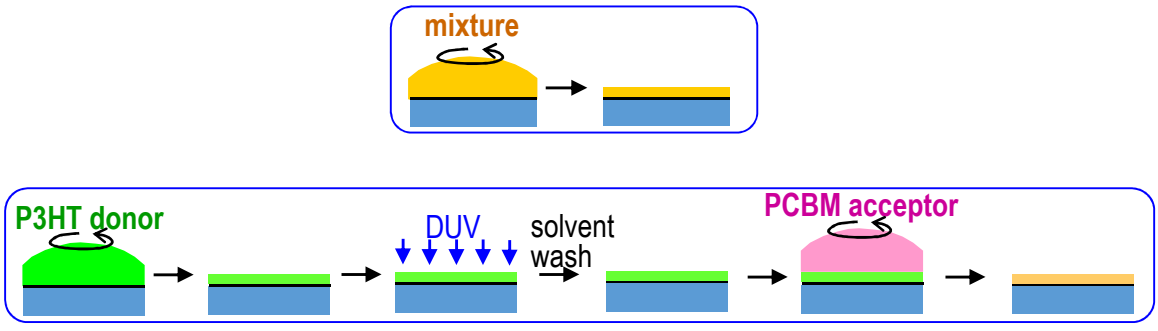

Figure 8: Schematic diagram for demixed biblend (top) and crosslinked back-infiltrated (bottom) active layer fabrication process.

Figure 9: Sol2A solar simulator from Newport. Certified to IEC 60904-9 2007 Edition.

Thin film active layers for UV-vis spectroscopy and PL measurements are similarly fabricated on a glass substrate without ITO, PEDT, or metals evaporated.

2.3.2 Solar simulation

The spectrum received at the sea level consists of a blackbody radiation from the Sun of around 5800K with an overall reduction in intensity from the scattering of air molecules and aerosol particles, and absorption by molecules in the atmosphere such as O_2 , H_2O and CO_2 constitute gaps in the spectrum. Albedo of the surface of the planet reflects a certain amount of light back into the atmosphere which then gets back-scattered to the planet and the accumulation of these effects is shown in figure 10.

Performance of solar cells are usually reported under solar illumination that has passed through one and a half of Earth's atmospheric air mass (AM1.5) which assumes the average thickness of atmosphere that sunlight has to pass through, given the angle of incident sunlight on a curved surface, to reach the surface of the Earth. In order to achieve this, a solar simulator[19] is used where a Xenon arc lamp is filtered with a 1.5G air mass filter, producing a very convincing simulation of sunlight, with low spectral mismatch, as shown in figure 10.

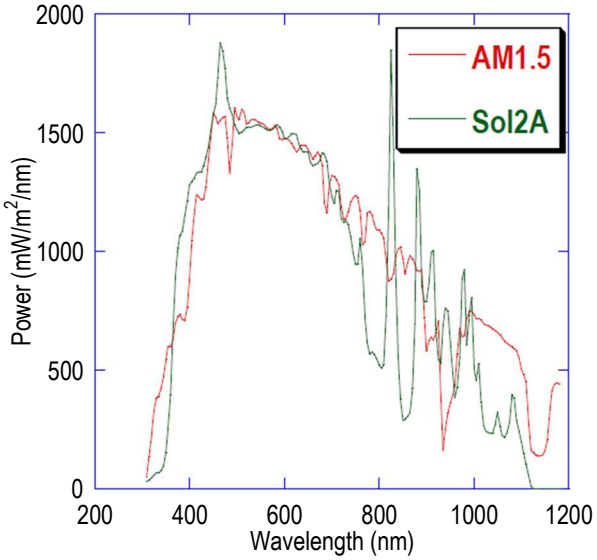

Figure 10: Power output from Sol2A with AM1.5 solar spectrum at sea level.

2.3.3 Device characterization

A solar cell is a diode which, under illumination, generates a reverse photocurrent. This reverse photocurrent ideally shifts the diode J-V curve down to produce a plot that is characteristic of a solar cell (figure 11). The maximum power that can be generated is referred to as the max power point and is achieved when the solar cell is worked at a corresponding max-power voltage. The efficiency of converting solar power received into electrical power is known as the power conversion efficiency (PCE) and can be extracted from the J-V curve as

$$\eta = \frac{P_{mpp}}{P_{in}} = \frac{J_{mpp}V_{mpp}}{P_{in}} = \frac{FF\,J_{sc}V_{oc}}{P_{in}} \tag{4}$$

where the fill factor, FF, is

$$FF = \frac{P_{mpp}}{J_{sc}V_{oc}} = \frac{J_{mpp}V_{mpp}}{J_{sc}V_{oc}} \tag{5}$$

The fill factor can depend on the resistance at zero bias, where space charges in the material impedes the extraction of charge carriers, requiring further external force, applied by the electric potential, to successfully remove the charge carriers from the active layer. If this issue is severe enough, it can spill over to affect the short circuit current (Jsc) as well, thus signifying

the importance of morphology in solar cell development. Other factors affecting PCE includes the open circuit voltage (Voc) which is affected by the difference in energy levels of the HOMO of the donor and the LUMO of the acceptor.

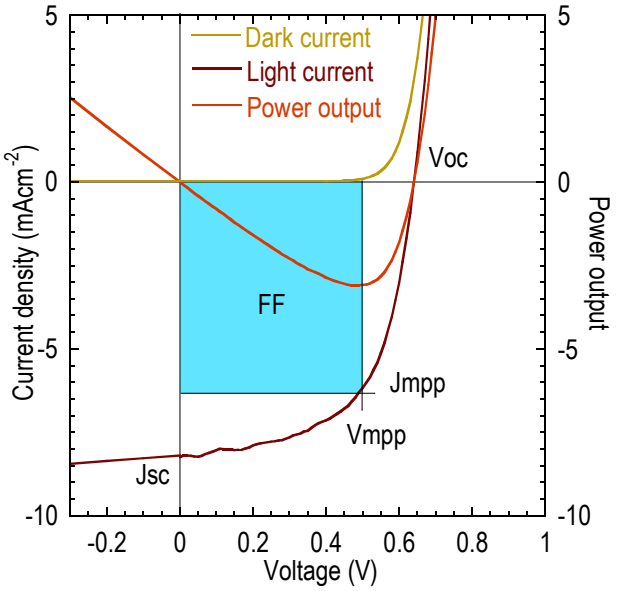

Figure 11: Typical J-V curve of a solar cell, produced under sweeping voltage, with power output curve.

2.3.4 Photoluminescence measurements

An excitation of a semiconducting material can lead to a relaxation process of luminescence where a photon is emitted (figure 12). When this excitation is in the form of an absorption of photon, it is called photoluminescence (PL).

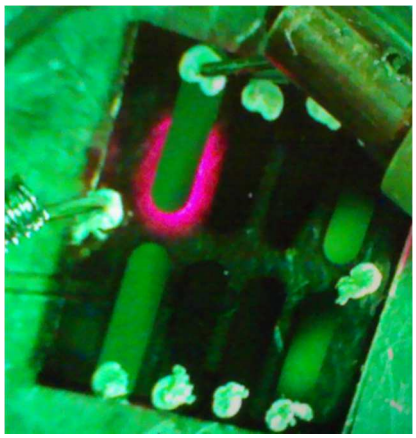

Figure 12: Electro-luminescence of a hole-only diode.

Although easily applied on solutions, on thin films this method of PL can also be done with the help of an integrating sphere[20] (figure 13). A laser is directed into the integrating sphere coated with a highly diffusive white material such as barium sulphate, which then baths the whole sphere in a sea of photons. If a photon manages to strike the thin film and be absorbed, an excitation occurs in the polymer material which creates an exciton and if this exciton is unable to reach the interface and dissociate within time, it can recombine and emit a photon. Through measurement of the intensity profile of the incident photons and emitted photons, we are able to deduce the efficiency of the recombination that occurs within the material.

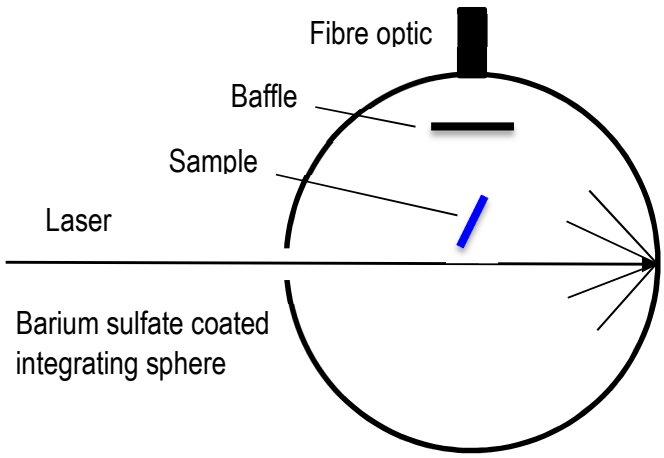

Figure 13: Schematic diagram of integrating sphere with laser not incident on sample.

Three sets of intensity profiles are collected, one without the thin film sample inside the sphere (a), one with the sample inside but off-centred and not incident on the laser (b), and a last one with the sample incident on the laser (c). These three sets of data yields information as shown in figure 14.

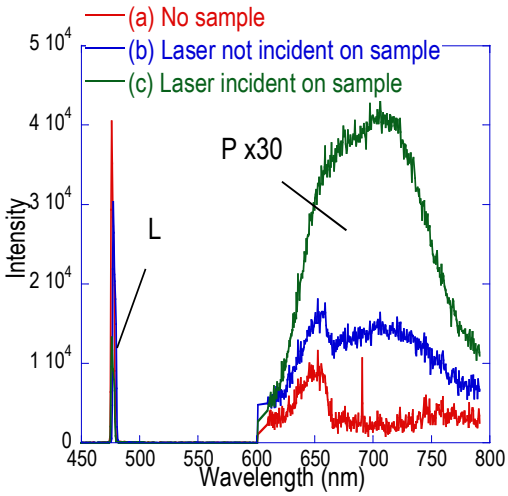

Figure 14: Typical plot of a PL intensity profile with the photoluminescence spectrum scaled up by 30. The three spectrums of a single thin film are shown here.

L is the area under the laser intensity profile and corresponds proportionally to the amount of unabsorbed light while P is the area under the emission profile and corresponds proportionally to the amount of emitted light. A large L therefore corresponds to a small P and vice versa. With these values, we are able to determine the fraction of scattered laser light that is absorbed, μ (eq 6), and the fraction of incident laser light that is absorbed, A (eq 7 and 8). From these, the external luminescence quantum efficiency, η, is obtained (eq 9 and 10).

$$L_b = L_a(1-\mu) \tag{6}$$

$$L_c = L_a(1-A)(1-\mu) \tag{7}$$

$$A = \left(1 - \frac{L_c}{L_b}\right) \tag{8}$$

$$L_c + P_c = (1-A)(L_b + P_b) + \eta L_a A \tag{9}$$

$$\eta = \frac{P_c - (1-A)P_b}{L_a A} \tag{10}$$

To measure how much recombination has been suppressed, a comparison is made between the luminescence quantum efficiency of a bulk heterojunction film with that of a pure single material film. This results in the quenching efficiency (QE) (eq 11).

$$QE = \frac{\eta_{pure\ film} - \eta_{BHJ}}{\eta_{pure\ film}} \times 100\% \tag{11}$$

3. Results and discussions

3.1 Photoluminescence

Photoluminescence is a powerful and integral tool to aid in the investigation of morphology. Its application is neither common nor straightforward in this field and therefore, the method for reading the measurements is aforehand mentioned. In this section, a model is proposed to account for the behaviour of the PL measurements of the active layer. However, bearing in mind that proper adjustments to offset the optical properties of equipment used (integrating sphere, fibre optic cable, etc) were not conducted, only relative comparisons should be used. As the laser wavelength (514 nm) used is directed to the absorption spectrum of the donor polymer, excitons formed is in the donor. Assuming an ideal device with a 100% exciton diffusion efficiency, a bilayer morphology would allow 20% of luminescence recombination to be quenched (10nm exciton diffusion length within a 50nm thick donor layer). In an ideal demixed biblend, where the phase separation of the donor is within twice the exciton diffusion length, the quenching efficiency would be 100%. In a back-infiltrated device, the quenching efficiency would then range from 20-100% depending on how much infiltration has occurred. In reality then, a deviation from the ideal in the demixed biblend would mean a less than optimal phase separation, while in the back-infiltrated active layer, a deviation would mean a similar less than optimal phase separation in the donor layer but also the possibility of an incomplete infiltration. Use of methods which are expected to provide better infiltration, such as use of a small molecular or more suitable solvent, are hence expected to improve QE of such back-infiltrated active layer.

3.2 Device characteristics

3.2.1 Characteristics of crosslinked donor matrix

The donor matrix was fabricated from spin-casting solution with the addition of 3% wt sFPA. The film was then exposed to 2 minutes of 254 nm DUV, washed with their respective solvents to create a sponge-like matrix. The sFPA molecule then inserts itself primarily into the CH bonds[12], however, at such a low concentration, the effects does not readily show itself on the UV-vis spectrum (figure 15) comparing non-crosslinked films to crosslinked films of equal thickness.

Retention rate reaches to 80% for both P3HT and PBDTTPD even for such low concentrations and greatly reduces the unnecessary repercussion of the crosslinkers. SCLC hole mobility of pure P3HT crosslinked matrix had a 4% drop with a mobility of 3.5×10^{-8} $m^2/(Vs)$, while for PBDTTPD, a 68% drop occurred with a mobility of 9.1×10^{-9} $m^2/(Vs)$.

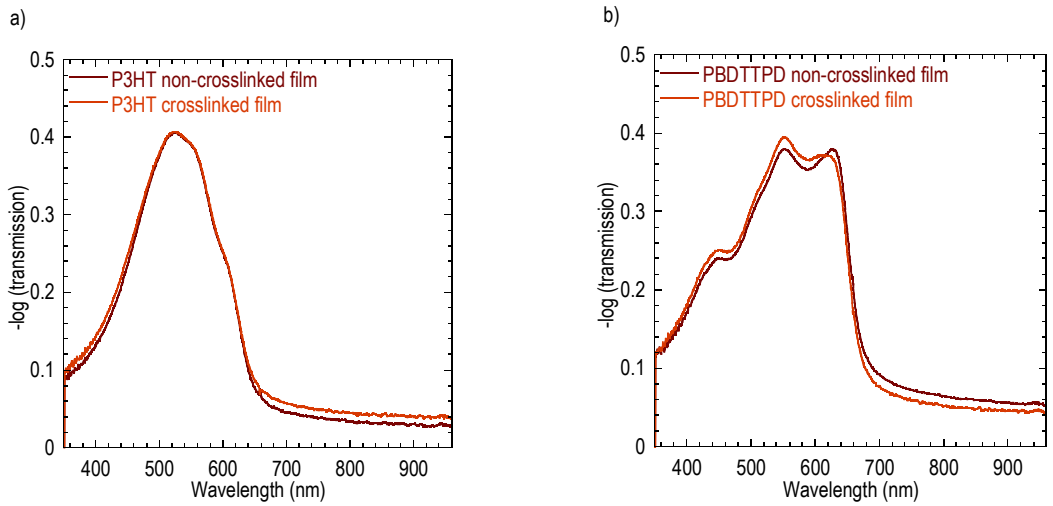

Figure 15: Uv-vis spectrum of a) P3HT non-crosslinked and crosslinked film. b) PBDTTPD non-crosslinked and crosslinked film.

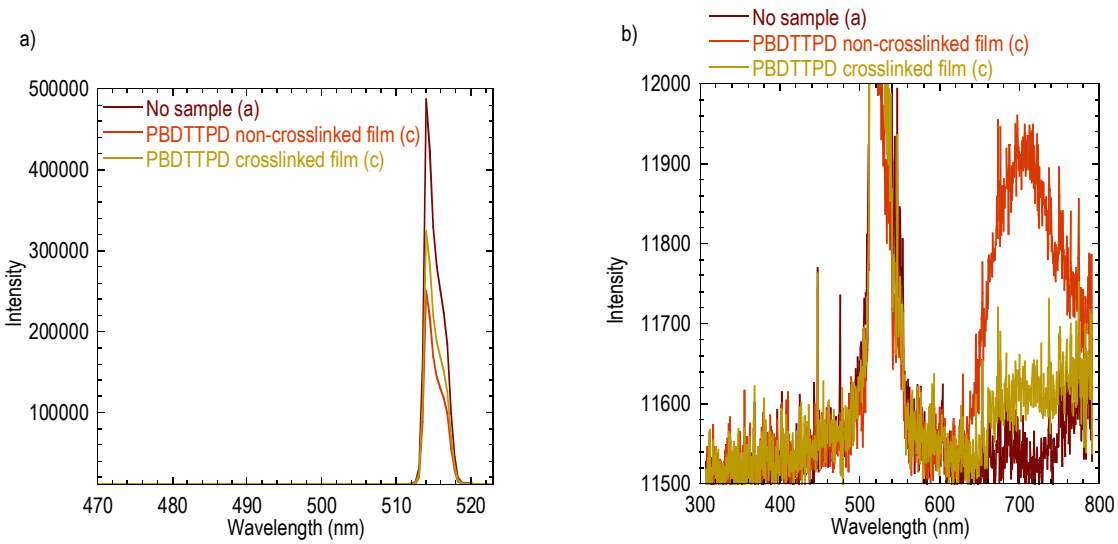

Figure 16: Intensity profile of no sample in the integrating sphere (a), PBDTTPD non-crosslinked (c) and crosslinked (c) film. a) Full laser intensity profile at 514 nm. b) Photoluminescence spectrum at 623-790 nm.

Since calculating the external luminescence quantum efficiency, η, is a very involved process requiring a total of 3 plots for a single measurement (refer to section 2.3.4), a simplified approach is attempted to visually explain the effects of crosslinker on η. Figure 16 shows the intensity profiles for no sample in the integrating sphere (a type (a) measurement), PBDTTPD non-crosslinked and crosslinked film of type (c) measurements. Type (b) measurements are left out for the sake of clarity. In figure 16a, laser attenuation represents absorption of that wavelength from the film (both direct and scattered). The non-attenuated laser profile is represented by no sample (a). In this example, a PBDTTPD non-crosslinked film showed slightly higher attenuation than its crosslinked counterpart but this may not always be the case since attenuation is also dependent on film thickness. Nevertheless, for identical materials, a higher attenuation should give a proportionally higher photoluminescence intensity spectrum. In figure 16b, the PBDTTPD non-crosslinked film does show higher photoluminescence but it is more than proportionally expected. So there is a quenching effect experienced by the introduction of the crosslinkers. This is not good for a pure film as it is proposed that traps and non-luminescent recombination losses could have resulted from the introduction of the crosslinkers[12]. It turns out that the QE for PBDTTPD film is 32.3% with η at 9.69% and 4.29% for non-crosslinked and crosslinked film respectively. QE for P3HT film is 36.8% with η at 2.90% and 1.84% for non-crosslinked and crosslinked film respectively. Hereafter, QE will be reported compared with their non-crosslinked and crosslinked pure film counterparts. These PL measurements are unadjusted data and absolute figures should not be cited.

3.2.2 P3HT:PCBM

P3HT:PCBM devices have been widely studied with morphologies of such blend devices taking on a self-assembled demixed state. Phase separation of P3HT:PCBM biblend devices were found to increase after thermal annealing[21] and crystallinity of P3HT and PCBM domains were also observed to increase after thermal annealing[22], improving absorbance and PCE. State of the art devices shows PCEs as high as 4.24%[11]. However, these biblend devices are sensitive to various fabrication conditions, such as the weight ratios of materials used, temperature during spin-coating and possible post-fabrication processes[23,24]. The introduction of crosslinking methodology provides us with more direct control over the domain sizes of the active layer and provides a robust morphology against film-processing conditions and degradation.

Figure 17 shows the –log (transmission) vs wavelength of an UV-vis spectrum through an active layer film. The demixed biblend BHJ is compared to a 50 nm crosslinked P3HT film and a PCBM back-infiltrated BHJ. From figure 17, a shift in peak position of P3HT in the BHJ is observed and results from disordering due to the presence of PCBM. Compared with the demixed biblend, a lower count in the region of 360-400 nm suggests that a thinner layer of PCBM was present in the back-infiltrated device. While being thinner, not a lot of PCBM was left on the surface of the matrix. This is indicated in the region of above 700nm where absorption from both materials is weak, as scattering from small molecules is also included in UV-vis spectrum. The thickness of the P3HT layer was also suggested to be reduced after back-infiltration with PCBM and may be due to the additional washing off of P3HT by the solvent chlorobenzene (CB) used in the PCBM solution. Despite these lower levels of absorption, the crosslinked device still performed beyond the demixed biblend.

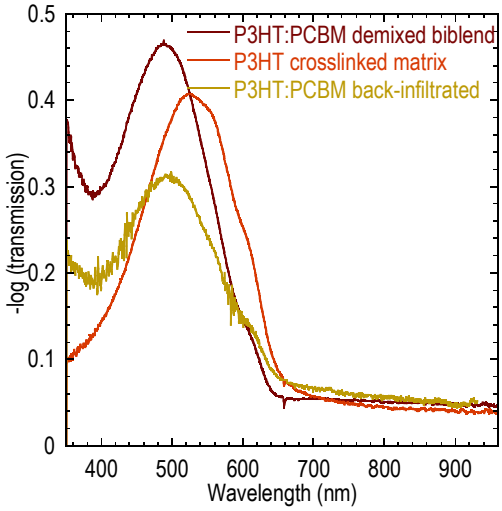

Figure 17: UV-vis spectrum of P3HT:PCBM demixed biblend, washed P3HT crosslinked matrix, and P3HT:PCBM back-infiltrated thin film.

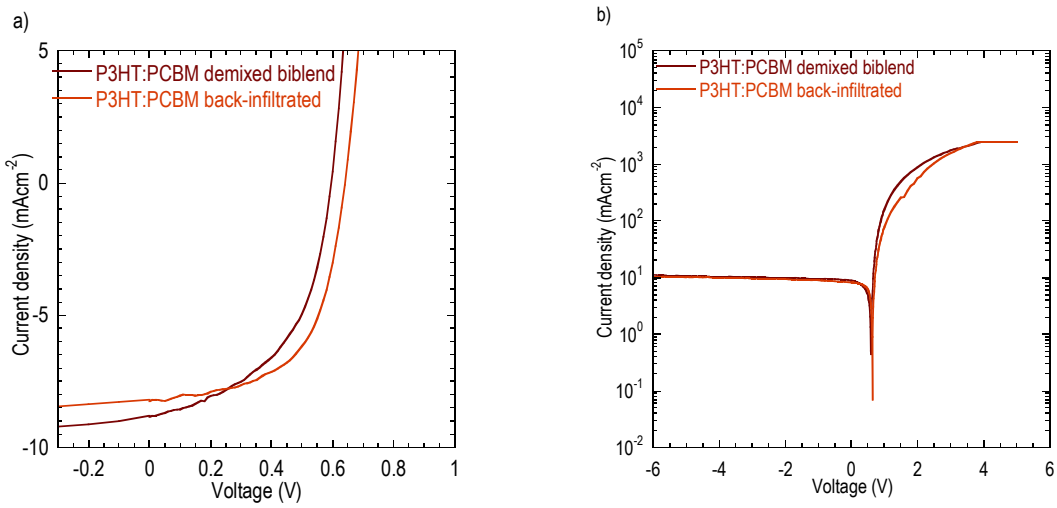

Figure 18: a) Linear-linear J-V curve of P3HT:PCBM demixed biblend and back-infiltrated device. b) Log-linear J-V curve.

Table 1: Output parameters of devices. *Unadjusted data.

	PCE (%)	Voc (V)	Jsc ($mAcm^{-2}$)	Vmpp (V)	Jmpp ($mAcm^{-2}$)	FF	QE* (%)
P3HT:PCBM demixed biblend	2.723	0.595	8.839	0.440	6.188	0.517	71.7
P3HT:PCBM back-infiltrated	3.139	0.641	8.248	0.480	6.540	0.594	43.3

J-V curve of the back-infiltrated device showed better FF and PCE, and slightly better Voc (figure 18a). Previous studies done on PCBM back-infiltration systems have yielded a 30% increase in PCE[13] largely due to an increase in Jsc. Our device was however lacking in this area, partly due to the reduced absorption, but still managed to achieve an increase in PCE due to an increase in Voc and the FF. Having a higher FF indicates that there is better extraction as can be seen in figure 18b where saturation current is reached early on. However, PL measurements indicate a less than optimal morphology. Compared to demixed biblend, QE of the back-infiltrated film is moderately lower, at zero bias. Since PCBM has shown to be a relatively good infiltrator, with little surface residual presence and good FF, The low QE can possibly be traced to the slightly coarser than ideal phase separation of P3HT donor matrix.

3.2.3 P3HT:PNDI

In 2012, Schubert et al. discovered an anticorrelation between the aggregation of PNDI in a P3HT:PNDI biblend device to its performance, and managed to achieve devices with PCEs up to 1.4%[25] through use of specific solvent compositions. They have also proposed that aggregation can lead to shortened exciton diffusion length. In fabrication with these materials, fine phase separations often lead to materials unable to form interpreting networks, hence produces isolated domains[26]. Our method of crosslinking is also able to prevent the aggregation of the acceptor polymer in the device and maintain a fine phase separation while maintaining better interpreting networks, improving on Voc and Jsc, and the performance of the device.

In this back-infiltration study, two types of PNDI were used, a purchased (Polyera ActivInk™ N2200) material with a high molecular weight (PNDI HMW) and an in-house produced polymer with a molecular weight of 20k (PNDI 20k). The absorption spectrum of both are shown in figure 19a with PNDI 20k having lower absorption and being slightly blue-shifted, In accordance with its shorter chain where PNDI 20k would create less energy states this results in a larger band gap and hence the blue shift. Figure 19b shows a UV-vis spectrum of the demixed biblend with a higher absorbance than their back-infiltrated counterparts. The lower absorption in the 500-600 nm region indicates less P3HT material in the back-infiltrated films while PNDI HMW back-infiltrated has similar thickness to the biblend.

SCLC mobility done for PNDI 20k showed a disappointing result of 5.6×10^{-10} $m^2/(Vs)$ which was a 2 order drop from PNDI HMW. Concern that contaminants might have been introduced as it was found in a wet state led to the low molecular weight (LMW) PNDI being sent for purification and drying. However, a back-infiltrated purified PNDI 20k device still showed a rather resistor-like behaviour.

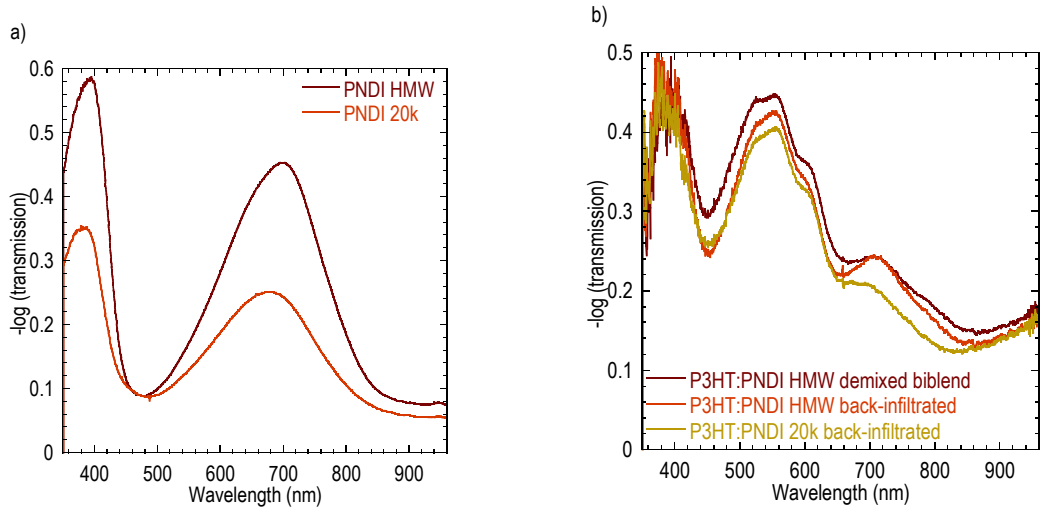

Figure 19: UV-vis spectrum of similar thickness of a) pure PNDI HMW and 20k film, b) P3HT:PNDI HMW demixed biblend, P3HT:PNDI HMW back-infiltrated and P3HT:PNDI 20k back-infiltrated films.

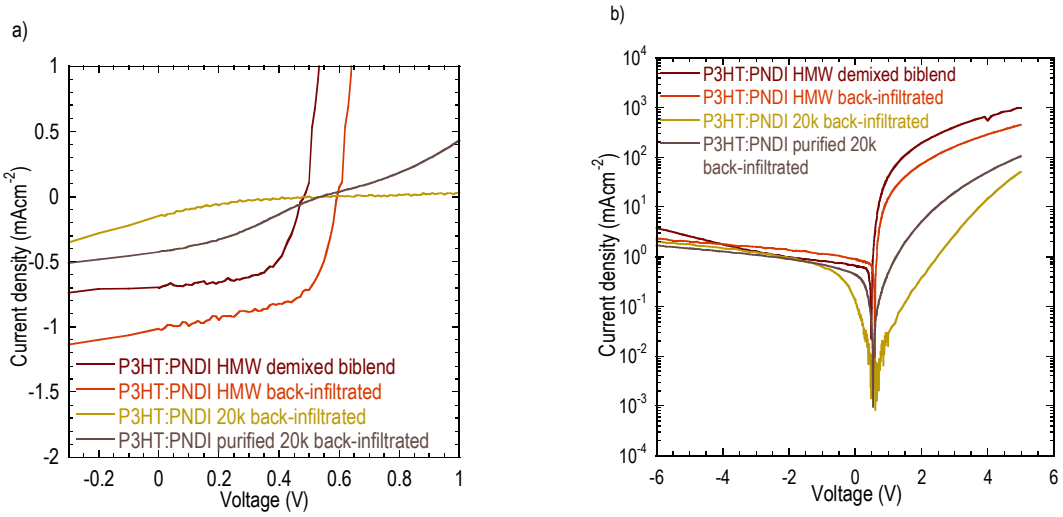

Figure 20: a) Linear-linear J-V curve of P3HT:PNDI HMW demixed biblend and back-infiltrated device, and P3HT:PNDI 20k non-purified and purified back-infiltrated device. b) Log-linear J-V curve.

Table 2: Output parameters of devices. *Unadjusted data.

	PCE (%)	Voc (V)	Jsc ($mAcm^{-2}$)	Vmpp (V)	Jmpp ($mAcm^{-2}$)	FF	QE* (%)
P3HT:PNDI HMW demixed biblend	0.205	0.483	0.704	0.380	0.539	0.602	43.3
P3HT:PNDI HMW back-infiltrated	0.346	0.602	0.969	0.490	0.706	0.593	19.2
P3HT:PNDI 20k back-infiltrated	0.013	0.494	0.146	0.219	0.061	0.184	36.8
P3HT:PNDI 20k purified back-infiltrated	0.205	0.483	0.704	0.380	0.539	0.602	-

PL measurements for these set of devices had conditions different from the study. The excitation laser used was of 475 nm but should not have great consequence, while η of P3HT crosslinked pure film was missed. To make up for this, η of non-crosslinked pure film was applied with the QE measured in later sets of P3HT non-crosslinked and crosslinked films. PL measurement of P3HT:PNDI 20k purified back-infiltrated film was also missed.

From figure 20a, the device performance of a PNDI HMW back-infiltrated system surpassed that of a demixed biblend in both Jsc and Voc, suffering slightly in FF, overall increasing PCE. PNDI 20k back-infiltrated devices fell in almost all parameters except for Voc when comparing with the biblend. It is suggested that the crosslinked matrix is able to create a finer phase separation for the PNDI, allowing for more efficient exciton diffusion to the donor-acceptor interface. An overall increase in charge carrier density was noted to be the primary factor for the increase in Jsc in PNDI HMW back-infiltrated, seen in figure 20b, as the saturation current was above that of the demixed biblend. PL done on the active matrix of a back-infiltrated PNDI 20k showed a higher quenching efficiency than that of a back-infiltrated PNDI HMW. This indicates that the smaller polymer was able to infiltrate better and vice versa.

In P3HT, QE of demixed biblend and crosslinked system were both moderately lower than the ideal and could indicate a thicker phase separation in the donor domain. To counter this in the crosslinked system, the exposure to the crosslinker activation DUV can be reduced to sacrifice retention rate for thinner phase separation. In all cases, PNDI HMW showed worse infiltration than its LMW variant. However, as observed above, performance of PNDI HMW fared better than LMW and possible balance towards infiltration and performance will be discussed later.

3.2.4 PBDTTPD:PCBM

While devices using P3HT as its donor material were able to utilize thermal annealing to develop its phase separation and absorbance due to P3HT's crystalline behaviour, other materials, which are mainly amorphous, cannot do so. Instead, other processing methods such as solvent annealing, which creates a slow drying condition, is used. Their end game is, however, still the same: to balance the phase separation requirements for efficient charge collection and exciton diffusion. Creating a donor matrix with our crosslinkers provides the possibility of having true percolation pathways which facilitates efficient charge collection, without compromising the need for a thin phase separation for efficient exciton dissociation.

Two solvents were used for the PCBM back-infiltration, chloroform (CF) and chlorobenzene, both spun to give equal thickness of PCBM, namely 40nm. In the UV-vis spectrum (figure 21) for the CF back-infiltrated active layer, the addition of the PCBM manifests in a higher count in the region around 400nm. In this UV-vis spectrum of the PCBM back-infiltrated active layer, there is a very clear example of scattering by small molecules lying on the surface. In the region above 700 nm, very little absorption occurs from both materials, and effects from scattering and reflection are most easily observed here. The CB back-infiltrated active layer showed a huge increase in this region and consequently, features belonging to PBDTTPD (the two peaks at 627 and 555 nm) were shifted up in counts without a correspondingly large lateral shift in wavelength. With roughly the same amount of PCBM present in both active matrix, this behaviour is attributed to the surface dwelling small molecules and consequently, infiltration from a CB solvent is less effective than a CF back-infiltrated active matrix. This is substantiated by PL measurements done on both active matrix, where the QE of the CF back-infiltrated was higher than that of CB, indicating better suppression of recombination of exciton which means better infiltration and possibly finer phase separation. While the solubility of PBDTTPD was lower in CF than CB[27] and solubility of PCBM in CF and CB being similar at 25 mg/mL[28], results showed a surprising deviation where the degree of PCBM infiltration was higher when back-infiltrated in CF than in CB.

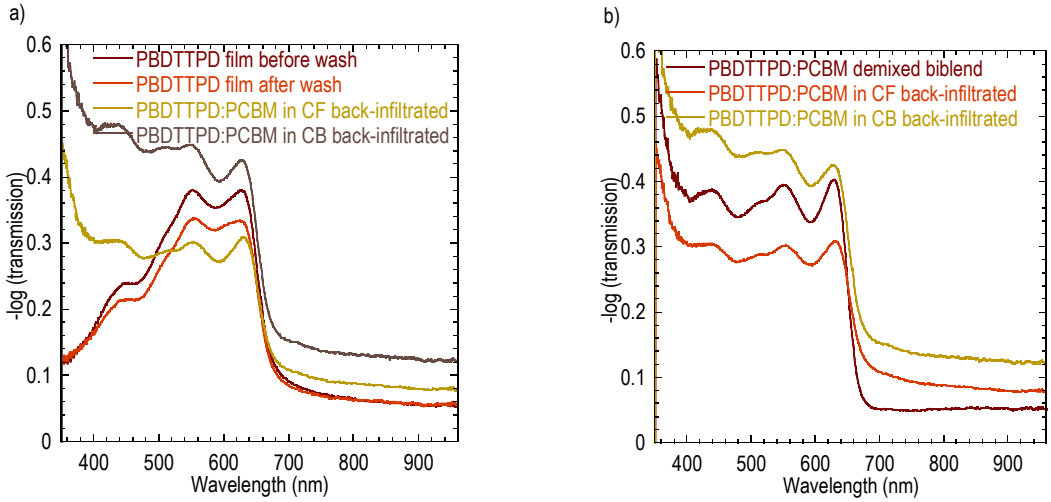

Figure 21: UV-vis spectrum of a) PBDTTPD film before and after washing, and PBDTTPD:PCBM in CF and CB back-infiltrated active layers. b) PBDTTPD:PCBM demixed biblend and PBDTTPD:PCBM in CF and CB back-infiltrated active layers

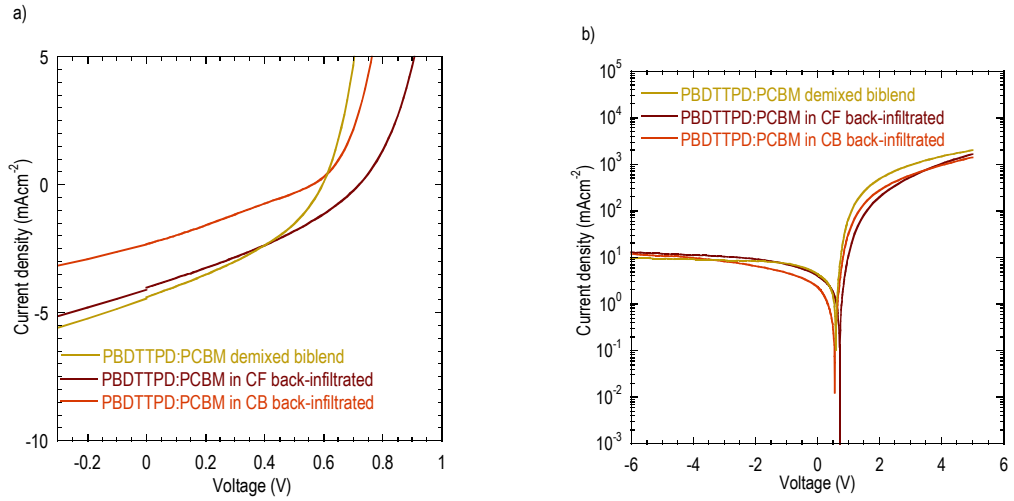

Figure 22: a) Linear-linear J-V curve of PBDTTPD:PCBM demixed biblend and PBDTTPD:PCBM in CF and CB back-infiltrated active layers. b) Log-linear J-V curve.

Table 3: Output parameters of devices. *Unadjusted data.

	PCE (%)	Voc (V)	Jsc ($mAcm^{-2}$)	Vmpp (V)	Jmpp ($mAcm^{-2}$)	FF	QE* (%)
PBDTTPD:PCBM demixed biblend	1.031	0.602	4.712	0.400	2.577	0.364	91.4
PBDTTPD:PCBM in CB back-infiltrated	0.349	0.562	2.324	0.280	1.246	0.267	67.7
PBDTTPD:PCBM in CF back-infiltrated	1.020	0.736	4.287	0.440	2.317	0.323	80.2

From figure 22a, against CB back-infiltrated device, CF back-infiltrated performed better in both Voc and Jsc, due partly to its higher QE which indicates better infiltration achieved. Against the demixed biblend, the CF back-infiltrated device had a higher Voc while Jsc was slightly worse, partly due to its worse absorption.

In all cases in figure 22b there was poor extraction as saturation current was reached only after the application of a substantial voltage. This poor extraction is also the cause of the poor FF and is most likely due to the poor mobility of PBDTTPD, which was 2 orders lower than that of PCBM. FF was worse for CF back-infiltrated and worst for CB and these two cases have reduced FF probably from the drop in hole mobility experienced by the PBDTTPD crosslinked matrix while the worst case of CB was additionally due to the poor infiltration that occurred.

PCE between the demixed biblend and back-infiltrated device was not too dissimilar (within 2% difference) and it is important to note that the blend ratios used in the biblend was PBDTTPD:1.5PCBM. This high level of PCBM was introduced to ensure the creation of an interpenetrating donor-acceptor morphology[27]. The thickness of PBDTTPD and PCBM in the back-infiltrated device was 52 and 40nm respectively. Since a crosslinked morphology provides better interpenetration and absorption coefficient of PCBM is low, optimization of material thickness can possibly lead to improvements in performance.

3.2.5 PBDTTPD:PNDI

While PNDI had a smaller band gap than PCBM, its lower LUMO levels meant that Voc with P3HT will be less than optimal. PBDTTPD has a HOMO level lower than that of P3HT while its LUMO was still necessarily more than 0.3 eV above that of PNDI, hence the two materials are proposed to complement well with each other on the energetic scale.

In this first study of PBDTTPD:PNDI system, two types of PNDI will be used, PNDI HMW and PNDI of 30k molecular weight (PNDI 30k). The UV-vis spectrum of the demixed biblend and the two crosslinked matrix are shown in figure 23. The spectrums do not have any major difference in features but being not a small molecule, scattering is reduced so even a simple bilayer with the same thickness of materials will produce similar spectrums. However, the spectrum can tell us that the PNDI HMW back-infiltrated active layer has less material in both PBDTTPD and PNDI HMW.

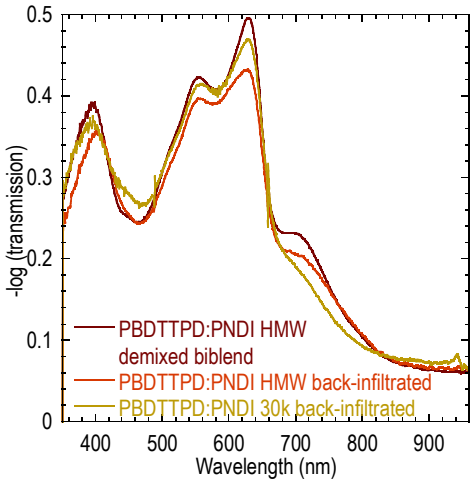

Figure 23: UV-vis spectrum of PBDTTPD:PNDI HMW demixed biblend and back-infiltrated and PBDTTPD:PNDI 30k back-infiltrated active layers.

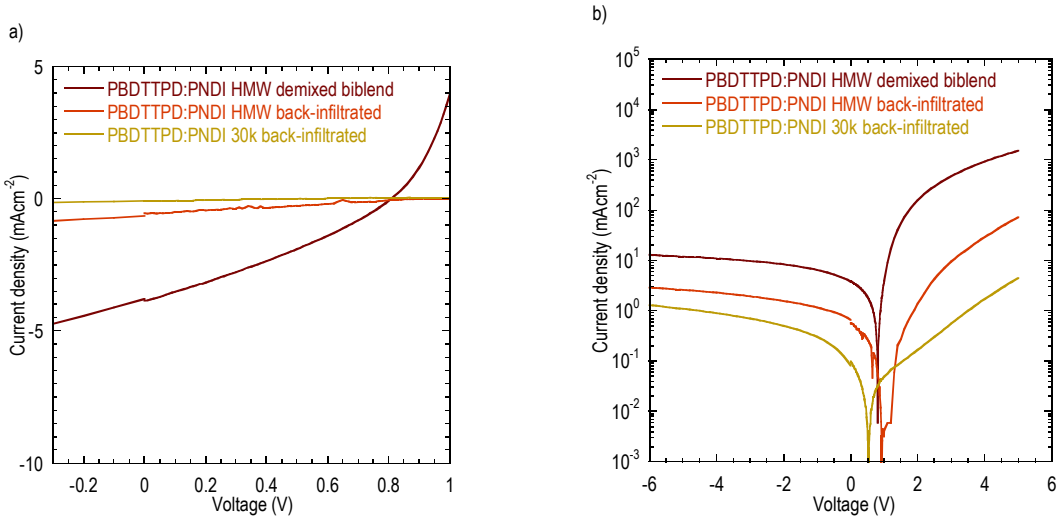

Figure 24: a) Linear-linear J-V curve of PBDTTPD:PNDI HMW demixed biblend and back-infiltrated and PBDTTPD:PNDI 30k back-infiltrated device . b) Log-linear J-V curve.

Table 4: Output parameters of devices. *Unadjusted data.

	PCE (%)	Voc (V)	Jsc ($mAcm^{-2}$)	Vmpp (V)	Jmpp ($mAcm^{-2}$)	FF	QE* (%)
PBDTTPD:PNDI HMW demixed biblend	0.963	0.809	3.866	0.460	2.093	0.308	93.2
PBDTTPD:PNDI HMW back-infiltrated	0.139	0.932	0.624	0.410	0.340	0.240	69.7
PBDTTPD:PNDI 30k back-infiltrated	0.012	0.530	0.098	0.280	0.042	0.224	83.1

Figure 24a shows us the poor performance of the back-infiltrated devices where parameters fell in almost all except for some Voc. Similar to the previous PBDTTPD:PCBM devices, PBDTTPD:PNDI devices showed poor FF. Jsc of the back-infiltrated device showed a drastic reduction when compared with the demixed biblend. When taken into account the drop in mobility of PBDTTPD after crosslinking, the Jsc was about 25% of that of demixed biblend. This coincides well with the model of a bilayer where the effective active layer is only 20nm, due to the short diffusion length of the exciton, when compared to the 100nm thick demixed biblend.

However, PL of PBDTTPD:PNDI HMW back-infiltrated active layer was not significantly lower than that of the demixed biblend, standing at 75% of the biblend's quenching efficiency, furthermore, QE was similar to PBDTTPD:PCBM in CB back-infiltrated active layer which meant similar levels of infiltration. Comparison between these devices showed consistent lower performance (PCE and FF) on part of the PNDI HMW polymer and would point the cause towards the lower electron mobility of PNDI. Back-infiltration of the smaller molecular weight polymer (PNDI 30k) once again showed higher QE over PNDI HMW.

In PBDTTPD demixed biblend, the QE reached near ideal levels which indicate a fine phase separation for the donor material, while for the crosslinked system, use of a low molecular weight PNDI or PCBM in CF also provided deep infiltration to lead QE near ideal levels. However, FF for back-infiltrated device fell and this would point us to a conclusion of a coarser phase separation in the acceptor domain.

3.3 Semiconducting behaviour of PNDI on molecular weight

Though the course of this study, it has been observed that the semiconducting behaviour of PNDI had a dependence on molecular weight. Mobility of semicrystalline semiconducting polymers are not entirely dependent on chain length for their mobility. This is especially true for low molecular weight variants where processing conditions can modify their mobilities by a hundred times[29]. As PNDI is shown to exhibit semicrystalline properties[25], SCLC electron mobility of PNDI are fit with a linear relationship to the molecular weight of the polymer to provide a simple estimation on the mobility with its molecular weight. This will allow the targeting of a certain molecular weight for the desired mobility, in order to improve infiltration.

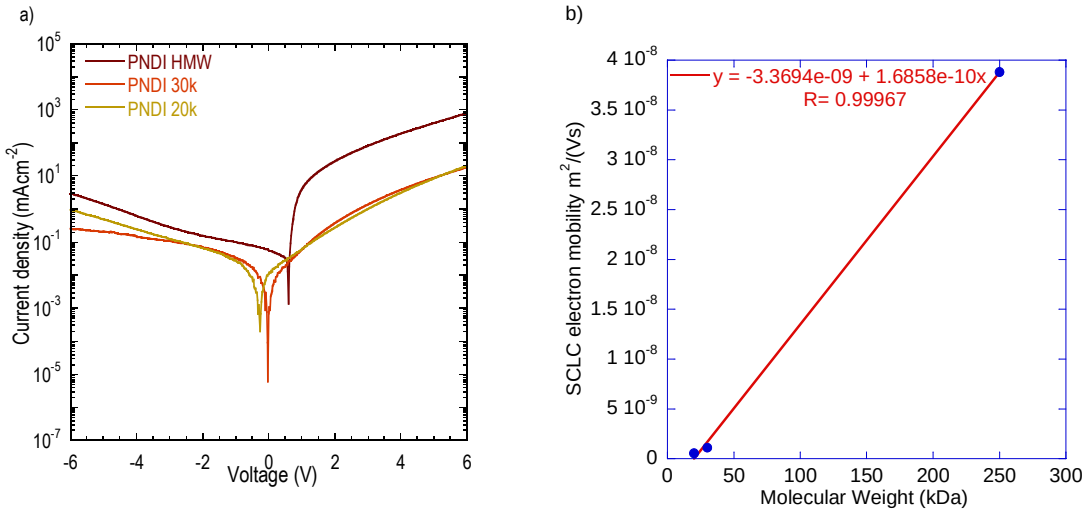

Figure 25: a) J-V curve of PNDI HMW, 20k and 30k. b) Linear fit of SCLC electron mobility against molecular weight.

3.4 Symmetricity

Symmetricity of mobilities between donor and acceptor materials have also to be taken into account. Free charge carriers generated in the middle of the active layer, if met with an asymmetric mobility between holes and electron, can lead to a build-up of charge carriers within the active layer as the faster rate of extraction of a type of charge carrier leaves a net of the opposite charge in the active layer. This space charge then impedes the flow of free charge carriers, requiring a higher potential to fully extract charge carriers, hence mobilities of similar orders are required for efficient extraction.

However, the generation of charge carriers are dependent on the absorption profile of the device with the depth of the device, and because of the orientation of the device and the optical interference from the reflected rays off the back of the device, an asymmetry is generated. In an active layer where reflection is minimized, this would lead to a larger optical profile in the front with the node at the back. Since the devices in this work are of superstrate structure, light enters from the hole collection electrodes and this corresponds to a hole collection electrode nearer to the bulk of the generated free charge carriers. As a result, electron have to travel a much larger distance to reach their electrode, and to aid them in their travels, an acceptor material with higher electron mobility should be deployed.

The optimal ratio for electron to hole mobility for superstrate structures was reported[30] to be around 10 ($\mu_e/\mu_h \approx 10$), with parallel increases in mobility giving, intuitively, higher FF and PCE. The massively low FF experienced by PBDTTPD:PNDI is within expectations of the combined low mobilities of PBDTTPD and PNDI.

Donor polymers have SCLC hole mobilities in the typical range of 10^{-9} to 10^{-8} $m^2/(Vs)$, hence optimal electron mobility would range from 10^{-8} to 10^{-7} $m^2/(Vs)$. Referring to figure 25, this would rule out the use of low molecular weight PNDIs below 100k molecular weight as suitable acceptors for current donor polymers. However, PNDIs between 100-250k molecular weight can be investigated for better infiltration while not sacrificing too much on performance.

4. Conclusion

Overall, crosslinking has provided quite a useful tool in improving morphology and performance of the solar cell. The drop in mobilities for crosslinked matrix was more than compensated by the improvements in morphology. The larger hole mobility drop for PBDTTPD crosslinked matrix only serves to provide an avenue for concocting a more suitable crosslinker, which will further improve cell performance.

Phase separation of donor and acceptor domains is still less than ideal and can be optimized for each specific active layer type, through adjustment of the extent of crosslinking in the donor phase. In all cases of PNDI HMW back-infiltration, lower levels of infiltration were observed. However, the drop was not enormous and optimising processing conditions is believed to be able to improve cell performance.

There were mixed reactions towards Jsc and FF as these two parameters depend on many factors, including morphology and mobilities. Voc followed trends according to their theoretical limit but for crosslinked back-infiltrated devices, an increase in Voc across the board was impressively observed but not understood. This increase is thought to be due to the presence of a slight bilayer on top of the crosslinked matrix which might provide better extraction of charge carriers with its larger cross-sectional area hence lower resistance.

Due to the optimal mobility ratio, it is expected that PNDI below 100k molecular weight would produce less than spectacular results due to its low mobility, while PNDI between 100-250k molecular weight should produce better infiltration without much loss in performance. Further breakthroughs in high electron mobility polymers will provide great excitement in the field of organic semiconductors where crosslinkers will still be able to aid in providing morphology support.

5. References

1. Morris, I., *Why the west rules-for now: The patterns of history and what they reveal about the future*. Profile books: 2010.
2. Wirth, H., Recent facts about photovoltaics in Germany. Fraunhofer ISE: January 7 2015.
3. Chamberlain, G., Organic solar cells: a review. *Solar cells* **1983,** *8* (1), 47-83.
4. Lizin, S.; Van Passel, S.; De Schepper, E.; Maes, W.; Lutsen, L.; Manca, J.; Vanderzande, D., Life cycle analyses of organic photovoltaics: a review. *Energy & Environmental Science* **2013,** *6* (11), 3136-3149.
5. Forrest, S. R., The path to ubiquitous and low-cost organic electronic appliances on plastic. *Nature* **2004,** *428* (6986), 911-918.
6. Brédas, J.-L.; Beljonne, D.; Coropceanu, V.; Cornil, J., Charge-transfer and energy-transfer processes in π-conjugated oligomers and polymers: a molecular picture. *Chemical Reviews* **2004,** *104* (11), 4971-5004.
7. Peumans, P.; Uchida, S.; Forrest, S. R., Efficient bulk heterojunction photovoltaic cells using small-molecular-weight organic thin films. *Nature* **2003,** *425* (6954), 158-162.
8. Brabec, C. J.; Zerza, G.; Cerullo, G.; De Silvestri, S.; Luzzati, S.; Hummelen, J. C.; Sariciftci, S., Tracing photoinduced electron transfer process in conjugated polymer/fullerene bulk heterojunctions in real time. *Chemical Physics Letters* **2001,** *340* (3), 232-236.
9. Tang, C. W., Two‐layer organic photovoltaic cell. *Applied Physics Letters* **1986,** *48* (2), 183-185.
10. Yu, G.; Gao, J.; Hummelen, J. C.; Wudl, F.; Heeger, A. J., Polymer photovoltaic cells: enhanced efficiencies via a network of internal donor-acceptor heterojunctions. *Science-AAAS-Weekly Paper Edition* **1995,** *270* (5243), 1789-1790.
11. Chi, D.; Qu, S.; Wang, Z.; Wang, J., High efficiency P3HT: PCBM solar cells with an inserted PCBM layer. *Journal of Materials Chemistry C* **2014,** *2* (22), 4383-4387.
12. Png, R.-Q.; Chia, P.-J.; Tang, J.-C.; Liu, B.; Sivaramakrishnan, S.; Zhou, M.; Khong, S.-H.; Chan, H. S.; Burroughes, J. H.; Chua, L.-L., High-performance polymer semiconducting heterostructure devices by nitrene-mediated photocrosslinking of alkyl side chains. *Nature materials* **2010,** *9* (2), 152-158.
13. Liu, B.; Png, R.-Q.; Zhao, L.-H.; Chua, L.-L.; Friend, R. H.; Ho, P. K., High internal quantum efficiency in fullerene solar cells based on crosslinked polymer donor networks. *Nature communications* **2012,** *3*, 1321.
14. Garcia-Belmonte, G.; Munar, A.; Barea, E. M.; Bisquert, J.; Ugarte, I.; Pacios, R., Charge carrier mobility and lifetime of organic bulk heterojunctions analyzed by impedance spectroscopy. *Organic Electronics* **2008,** *9* (5), 847-851.
15. Dang, M. T.; Hirsch, L.; Wantz, G., P3HT: PCBM, best seller in polymer photovoltaic research. *Advanced Materials* **2011,** *23* (31), 3597-3602.
16. Yan, H.; Chen, Z.; Zheng, Y.; Newman, C.; Quinn, J. R.; Dötz, F.; Kastler, M.; Facchetti, A., A high-mobility electron-transporting polymer for printed transistors. *Nature* **2009,** *457* (7230), 679-686.
17. Zou, Y.; Najari, A.; Berrouard, P.; Beaupré, S.; Réda Aïch, B.; Tao, Y.; Leclerc, M., A thieno [3, 4-c] pyrrole-4, 6-dione-based copolymer for efficient solar cells. *Journal of the American Chemical Society* **2010,** *132* (15), 5330-5331.
18. Qin, R.; Li, W.; Li, C.; Du, C.; Veit, C.; Schleiermacher, H.-F.; Andersson, M.; Bo, Z.; Liu, Z.; Inganas, O., A planar copolymer for high efficiency polymer solar cells. *Journal of the American Chemical Society* **2009,** *131* (41), 14612-14613.
19. Oriel® Sol2A™ Class ABA Solar Simulators. Newport: 2007.

20. de Mello, J. C.; Wittmann, H. F.; Friend, R. H., An improved experimental determination of external photoluminescence quantum efficiency. *Advanced materials* **1997,** *9* (3), 230-232.
21. Dennler, G.; Scharber, M. C.; Brabec, C. J., Polymer‐Fullerene bulk‐heterojunction solar cells. *Advanced Materials* **2009,** *21* (13), 1323-1338.
22. Yang, X.; Loos, J.; Veenstra, S. C.; Verhees, W. J.; Wienk, M. M.; Kroon, J. M.; Michels, M. A.; Janssen, R. A., Nanoscale morphology of high-performance polymer solar cells. *Nano letters* **2005,** *5* (4), 579-583.
23. Tremolet de Villers, B.; Tassone, C. J.; Tolbert, S. H.; Schwartz, B. J., Improving the reproducibility of P3HT: PCBM solar cells by controlling the PCBM/cathode interface. *The Journal of Physical Chemistry C* **2009,** *113* (44), 18978-18982.
24. Liu, Z.; Lee, E.-C., Efficiency improvement in fullerene-layer-inserted organic bulk-heterojunction solar cells. *Journal of Applied Physics* **2012,** *111* (2), 023104.
25. Schubert, M.; Dolfen, D.; Frisch, J.; Roland, S.; Steyrleuthner, R.; Stiller, B.; Chen, Z.; Scherf, U.; Koch, N.; Facchetti, A., Influence of Aggregation on the Performance of All‐Polymer Solar Cells Containing Low‐Bandgap Naphthalenediimide Copolymers. *Advanced Energy Materials* **2012,** *2* (3), 369-380.
26. Zhou, N.; Lin, H.; Lou, S. J.; Yu, X.; Guo, P.; Manley, E. F.; Loser, S.; Hartnett, P.; Huang, H.; Wasielewski, M. R., Morphology‐Performance Relationships in High‐Efficiency All‐Polymer Solar Cells. *Advanced Energy Materials* **2014,** *4* (3).
27. Aïch, B. R.; Lu, J.; Beaupré, S.; Leclerc, M.; Tao, Y., Control of the active layer nanomorphology by using co-additives towards high-performance bulk heterojunction solar cells. *Organic Electronics* **2012,** *13* (9), 1736-1741.
28. Kronholm, D.; Hummelen, J., Fullerene-based n-type semiconductors in organic electronics. *Material Matters* **2007,** *2*, 16-20.
29. Kline, R. J.; McGehee, M. D.; Kadnikova, E. N.; Liu, J.; Frechet, J. M.; Toney, M. F., Dependence of regioregular poly (3-hexylthiophene) film morphology and field-effect mobility on molecular weight. *Macromolecules* **2005,** *38* (8), 3312-3319.
30. Liu, B.; Png, R. Q.; Tan, J. K.; Ho, P. K., Evaluation of Built‐In Potential and Loss Mechanisms at Contacts in Organic Solar Cells: Device Model Parameterization, Validation, and Prediction. *Advanced Energy Materials* **2014,** *4* (4).

6. Appendix

A1. SCLC mobility

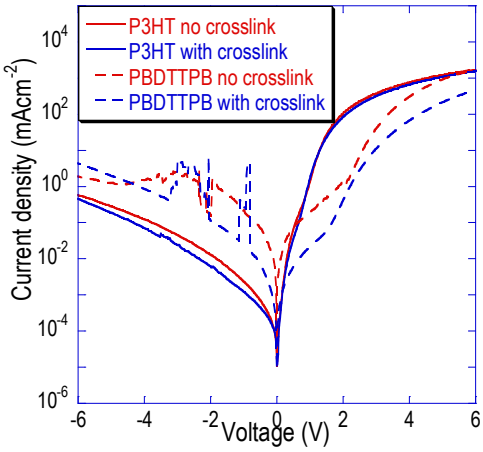

Fig A1: J-V curves of P3HT and PBDTTPD non crosslinked and crosslinked films.

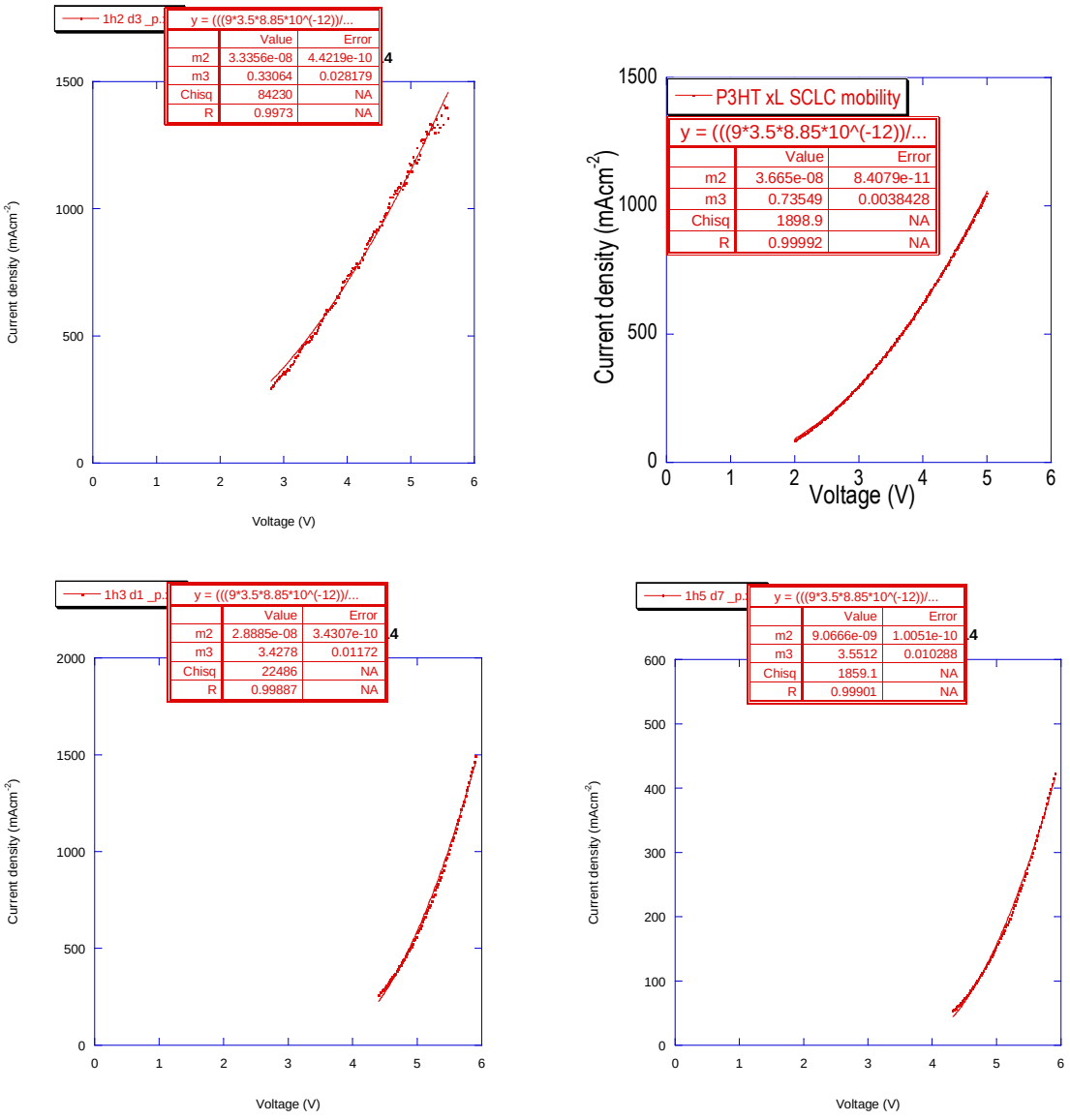

Fig A2: J-V curve fitting with the Mott-Gurney law. P3HT non crosslinked film (top left). P3HT crosslinked film (top right). PBDTTPD non crosslinked film (bottom left). PBDTTPD crosslinked film (bottom right).

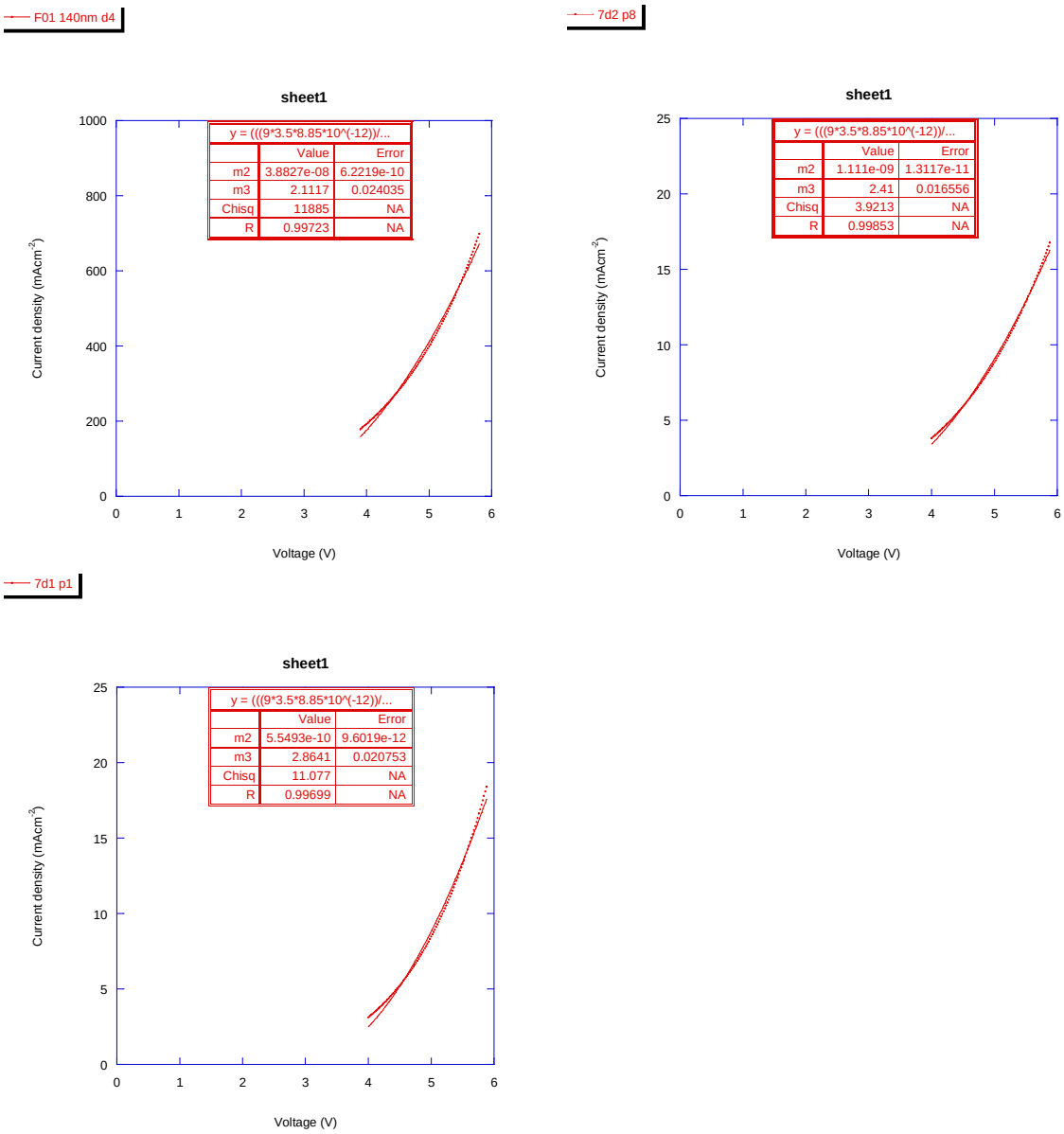

Fig A3: J-V curve fitting with the Mott-Gurney law. PNDI HMW (top left). PNDI 30k (top right). PNDI 20k (bottom right).

A2. Device solution weight ratios and film thickness

P3HT:PCBM biblend at (1:0.8) targeted at 90 nm, back-infiltrated at (50 nm:40 nm)

P3HT:PNDI biblend at (1:1) targeted at 100 nm, back-infiltrated at (50 nm:50 nm)

PBDTTPD:PCBM biblend at (1:1.5) targeted at 100 nm, back-infiltrated at (55 nm:45 nm)

PBDTTPD:PNDI biblend at (1:1) targeted at 100 nm, back-infiltrated at (50 nm:50 nm)

A3. Photoluminescence

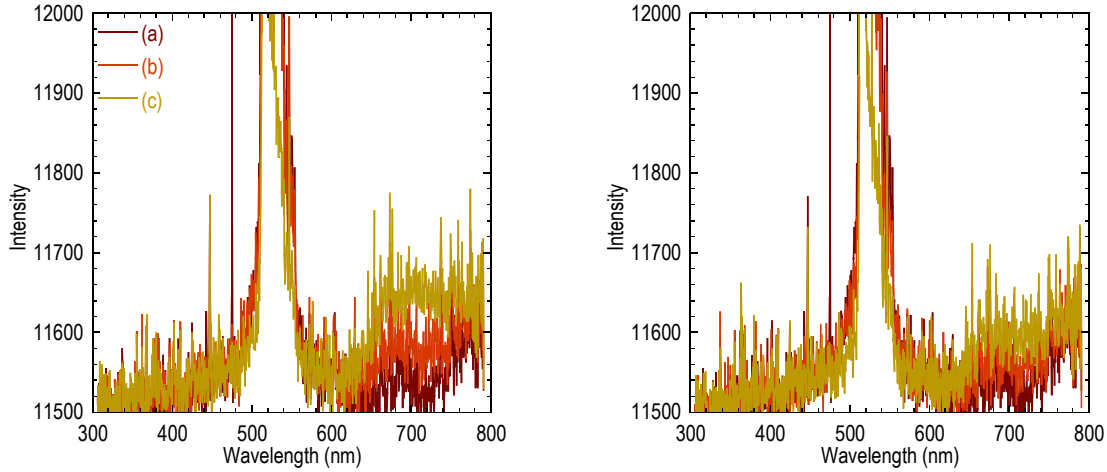

Fig A4: PL of P3HT non-crosslinked film (left) and crosslinked film (right).

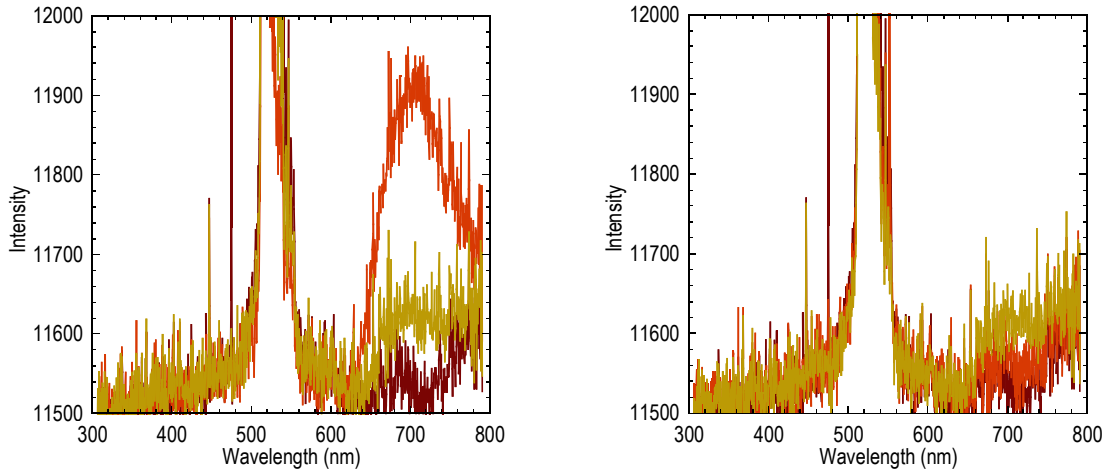

Fig A5: PL of PBDTTPD non-crosslinked film (left) and crosslinked film (right).

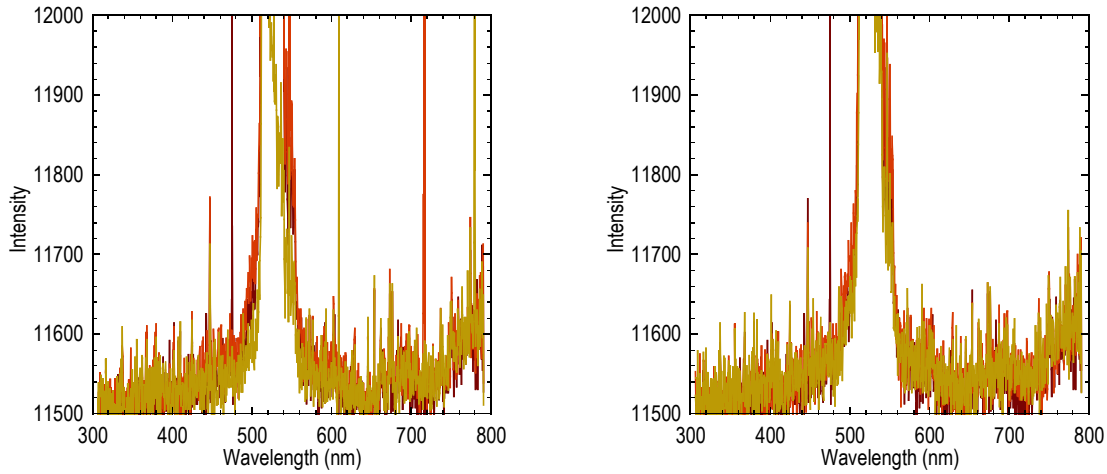

Fig A6: PL of P3HT:PCBM demixed biblend film (left) and back-infiltrated film (right).

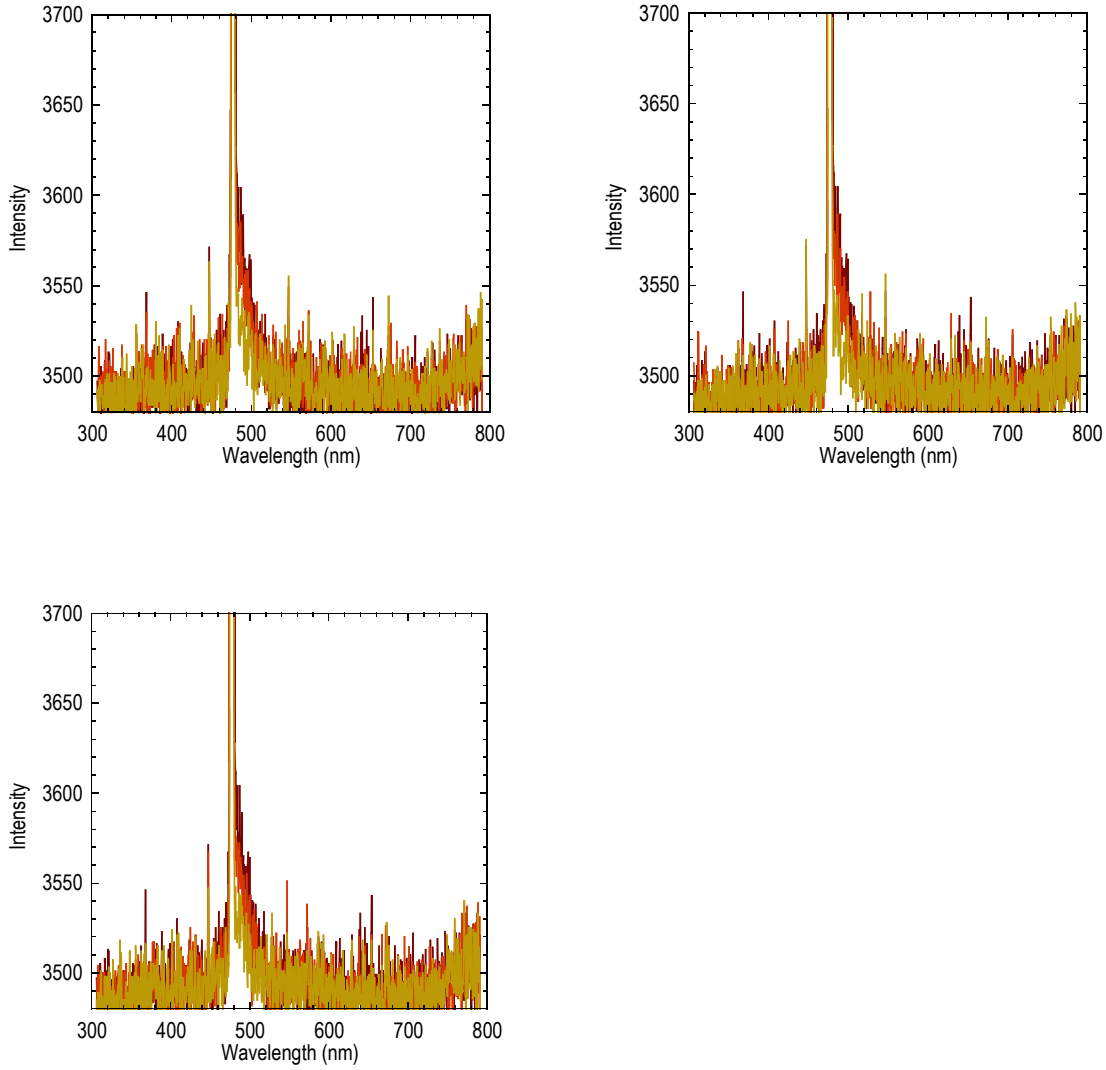

Fig A7: PL of P3HT:PNDI HMW demixed biblend film (top left), back-infiltrated film (top right) and P3HT:PNDI 20k back-infiltrated film (bottom left).

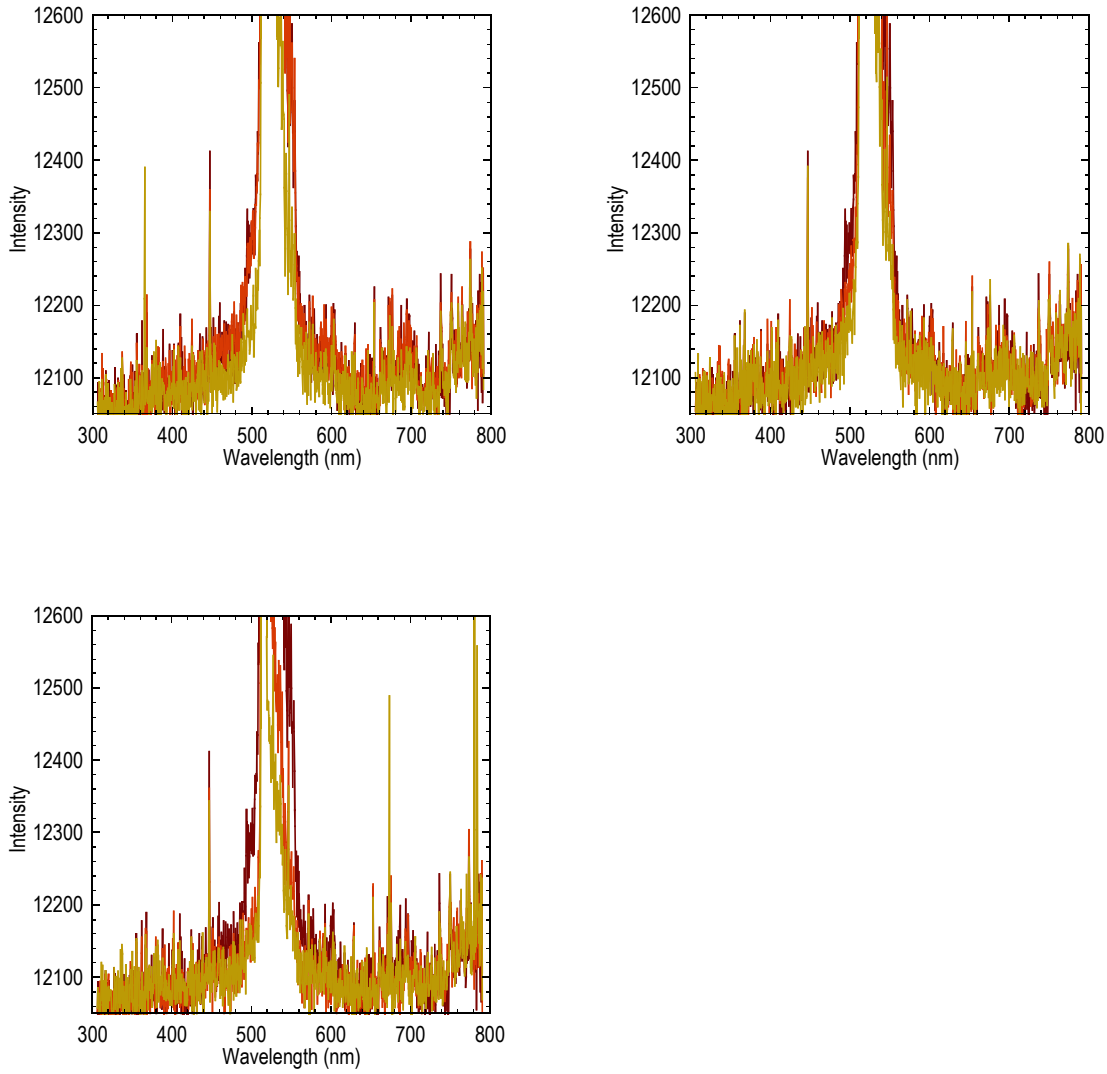

Fig A7: PL of PBDTTPD:PCBM demixed biblend film (top left), in CF back-infiltrated film (top right) and in CB back-infiltrated film (bottom left).